Starburst Galaxies

Ivana Orlitova

Contents

Abstract The rate of star formation varies between galaxy types and evolves with redshift. Most stars in the universe have formed in episodes of an exceptionally high star-forming activity, commonly called a starburst. We here summarize basic definitions and general properties of starbursts, together with their observational signatures. We overview the main types of starburst galaxies both in the local universe and at high redshift, where they were much more common. We specify

I. Orlitova (✉)
Astronomical Institute of the Czech Academy of Sciences, Ondřejov, Czechia
e-mail: orlitova@asu.cas.cz

similarities and differences between the local and distant samples and specify the possible evolutionary links. We describe the role of starburst galaxies in the era of cosmic reionization, relying on the most recent observational results.

1 Star Formation and Starburst

The rate of star formation is one of the basic characteristics of a galaxy. The stellar content and stellar age provide observational signatures that allow us to derive the history of galaxy evolution. The star formation rate (SFR), defined as the stellar mass increase per unit time, dM_*/dt, can range from zero, such as in gas-poor elliptical galaxies, to hundreds or thousands of solar masses per year ($M_\odot$ year^{-1}) in the most vigorously star-forming galaxies. For illustration, the Milky Way (MW) forms stars at a rate of less than $1\,M_\odot$ year^{-1}. Star formation (SF) can be continuous and more-or-less regular, or it can consist of short and intense bursts separated by long intervals of quiescence. Understanding how galaxies make stars and what drives the differences between them is an active field of research. We will here overview the main observational methods and results, focusing specifically on galaxies that undergo a burst of star formation.

The SFR alone may not be a sufficient parameter to characterize how important is the SF in a given galaxy. In principle, the more massive the galaxy, the larger the SFR can be, if enough cold gas ($\sim 10\,K$) is available. It is convenient to define relative quantities that allow a better comparison between galaxies. By factoring out the galaxy stellar mass, we obtain the specific star formation rate (sSFR), the SFR per unit mass. The sSFR is proportional to the birthrate parameter b, the ratio of the current SFR to the average past SFR [1]. Another useful quantity is the surface density of star formation, Σ_{SFR}, which measures the SFR per unit area and which correlates with the gas surface density Σ_{gas} (combined atomic H I and molecular H$_2$). This relation is commonly called 'Schmidt-Kennicutt' and has been discussed in detail in Kennicutt's review [1]. An updated picture, using recent multi-wavelength data, clarifies that the relation is mainly driven by molecular Σ_{H_2} [2, 3].

Star formation proceeds through the assembly of cold gas into dense clouds which eventually undergo gravitational collapse once they attain masses of $\sim 10^6\,M_\odot$ and sizes up to $100\,pc$. What drives this gas compression and what triggers the SF is a subject of many discussions as we will present in the following sections (shock waves, stellar density waves such as bars or tidal interactions). How is the available gas converted into stars is then described by the SFR efficiency $\epsilon = SFR/M_{gas}$ (definition used in extragalactic studies, different from that for individual clouds in the MW). The inverse of the efficiency is called the depletion time, which states how long can the galaxy continue forming stars at the current rate with the given mass of atomic H I and molecular H$_2$. A large spread of efficiencies is observed in local galaxies, with an average of $\sim 5\%$ per 10^8 years [1–3], corresponding to a depletion time of $2\,Gyr$ (which can in reality be a factor of two longer due to recycling of gas from stellar winds).

Fig. 1 Starburst region 30 Doradus (also known as Tarantula nebula) in the Large Magellanic Cloud. The multi-colour UV and optical image was obtained using the Hubble Space Telescope and shows the central concentration of young stars (called R136) in the NGC 2070 star cluster, which is situated at the core of the nebula. R136 contains several O stars and Wolf-Rayet stars and produces most of the energy that makes the 30 Doradus visible. Credit: NASA/ESA

When a galaxy undergoes an exceptionally intense phase of SF, we speak of a starburst (Fig. 1). A starburst galaxy is thus not a separate class and it is rather an evolutionary phase in the life of a galaxy. The starburst activity may not be uniformly spread across the galaxy. While global starbursts preferentially occur in dwarfs, the starbursts in massive galaxies are usually localized in a small volume, most often in the circumnuclear region, where 10^8–$10^{10}\,M_\odot$ of gas is confined to a radius of < 1 kpc. The reasons behind the vigorous star formation are not yet fully understood and we will mention here the main scenarios. The most appealing is the effect of gravitational interaction between galaxies, ranging from a close passage to a complete merger (from pioneering papers such as [4, 5] to recent observations [6] and simulations [7]). The tidal forces perturb the orbits of gas and stars and enable the gas flow toward the galaxy center. However, it is not yet clear whether such an encounter is a necessary condition (some starburst galaxies seem to be isolated), nor whether the encounter is a sufficient condition (tidal forces between dwarf galaxies are modest). A similar transfer of gas is also possible by the action of gravitational instabilities such as stellar bars [8, 9]. Subsequently, local dynamical processes including the pressure, the local velocities, the starlight and self-gravitation decide on the future of the gas clouds (as reviewed by [9, 10]). The accumulation of gas in the central parts is essential for yet another phenomenon: feeding of the active galactic nucleus (AGN), i.e. the central galactic region dominated by a supermassive

black hole. Indeed, a simultaneous AGN and starburst activity exists in numerous galaxies, as we will describe in the following sections. It is still a matter of debate if the coexistence is coincidental or if there is a causal relationship [11]. If no apparent causes of starburst are visible, we can speculate about the time delays between different phenomena or invoke the role of shock waves due to preceding star formation and supernova explosions [9, 12].

There is no unique and rigorous definition of a starburst, and a good definition is being discussed in the literature still today [3, 13, 14]. The classical definition is related to the amount of gas in the galaxy and the maximum lifetime of the starburst: the galaxy would consume all of its remaining gas in a limited time were the SFR constant. If this consumption (depletion) time is much shorter than the age of the universe, then we define the galaxy as a starburst. In other words, the efficiency of SF must be at least an order higher than in an average local galaxy [1]. However, the problem with this definition is the uneven gas fraction in different galaxy types. The depletion time in a massive, gas-poor galaxy can be short, yet without any sensible reason to call it a starburst. An alternative definition is based on the birthrate parameter: one can estimate the time that the galaxy would need in order to create all of its existing stars at the present SFR. This approach represents a disadvantage for massive galaxies where the timescales to reproduce their stellar mass are excessively long. Moreover, both of these approaches have a built-in redshift dependence—the varying age of the universe changes the quantitative meaning of starburst parameters at each redshift [13]. One therefore has to be careful what is meant by a starburst in each study. Heckman [13] proposed to define a starburst based on Σ_{SFR}, which treats equivalently both nearby and high-redshift galaxies. High Σ_{SFR} implies large surface densities of both gas and stellar mass [1]. As a consequence, such regions will have a high gas pressure, a high rate of mechanical energy deposition and a high density of radiant energy. Σ_{SFR} is hence directly linked to the galaxy physical properties.

The definition of a starburst may have to stay loose, we can nevertheless require a parallel application of several criteria, and, in addition, add a qualitative requirement that the starburst must have a global impact on its host galaxy evolution—powerful outflows, significant mass fraction transformed to stars, disturbed structure, enhanced luminosity, etc. Typically, authors require $b \geq 3$ or $b \geq 10$ to select starburst galaxies [15, 16]. The undisputed starbursts have durations of 10^7–10^8 years and $\Sigma_{SFR} \sim 1$–$100 \, M_\odot \, \text{year}^{-1} \, \text{kpc}^{-2}$, which exceeds Σ_{SFR} of the MW by several orders of magnitude [13]. The most extreme of them form stars with efficiencies close to 100% per 10^8 year [1]. What is certain is that the upper bound for efficiency must be set by causality—conversion of the entire self-gravitating gas reservoir into stars in one dynamical time.

Starbursts (defined by $b \geq 3$) currently form 20% of the present-day massive stars [13], representing a non-negligible baryonic constituent of the local universe (if $b \geq 10$ is considered, the fraction drops to 3%). Because of their young age, they contain large numbers of massive stars and X-ray binaries, and they thus offer unique opportunities for studying the high-mass objects and their feedback in the form of mechanical energy (winds, jets) and energetic photons (ultraviolet, X-rays).

The collective action of stellar winds, supernovae and jets drives powerful outflows of gas on the galactic scale. Also known under the name superwinds, the large-scale outflows transport material, including heavy elements, to the intergalactic medium (IGM). The localized starburst hence directly affects a large volume of space. Starburst galaxies were much more frequent in the early universe than they are today and they played an important role in shaping the IGM throughout the history of the universe. Besides, they were responsible for forming most of the stars in the universe as they were the building blocks of present-day galaxies. SF then sharply dropped after redshift $z \sim 2$ (i.e. age of the universe $\sim 3\,\mathrm{Gyr}$). The first starbursts also played yet another role in cosmology: the ultraviolet radiation of young massive stars was probably responsible for converting the IGM from neutral to ionized in the first billion years after the Big Bang (so called Cosmic Reionization).

The goal of the following sections is to provide a basic description of how are starbursts observed and how the observational methods lead to their "classification" both at low and high redshift. Section 2 describes the starburst signatures at various spectral wavelengths. Section 3 overviews the major starburst galaxy types in the local universe. Section 4 presents the high-redshift galaxy classes, all detected thanks to the starburst signatures. Section 5 focuses on the role of starburst galaxies in the cosmic reionization. Finally, Sect. 6 brings concluding remarks and future prospects, including the observational facilities that are in preparation.

2 Observational Signatures of a Starburst

Star formation manifests itself by a variety of features across a large portion of the electromagnetic spectrum. We observe the direct starlight of young stars as well as the light reprocessed by interstellar gas and dust. Detailed and insightful reviews of SFR indicators were provided by Kennicutt [3] and Calzetti [17].

2.1 Ultraviolet and Optical Continuum

The UV and optical light of young stellar populations is dominated by massive stars with the lifetimes of 10^6–10^8 years. The O and B stars produce most of their energy in the far-ultraviolet (FUV) band, including a large fraction at Lyman continuum wavelengths ($\lambda < 912\,\text{Å}$), capable of ionizing hydrogen atoms. In parallel, massive stars drive powerful stellar winds that affect kinematics of the interstellar medium (ISM) and produce specific spectral features. The importance of the UV observations in starbursts was demonstrated by the International Ultraviolet Explorer (*IUE*) satellite, operating for almost 20 years before the end of the twentieth century. The *IUE* was followed by the Far Ultraviolet Spectroscopic Explorer (*FUSE*), the Galaxy Evolution Explorer (*GALEX*), and the Hubble Space Telescope (*HST*). Thanks to the *IUE*, the first UV catalogue of stellar types was issued in 1985 [18].

In the dust-poor case, the bright UV continuum is a prominent signature of
the young massive stars, i.e. of a starburst. The bright UV is also observable for
high-redshift galaxies and represents one of the major methods of galaxy detection
(Sect. 4.1, Fig. 6). Furthermore, empirical relations exist between the SFR and the
UV luminosity, and therefore both FUV and near-UV (NUV) luminosities serve as
SFR estimators [17]. Nevertheless, the total SFR estimation must ideally take into
account the effect of dust. The dust efficiently reprocesses the UV light into infrared
(IR) radiation (see Sect. 2.5). Therefore, combined UV and IR measurements
provide a more precise determination of the galaxy SFR [17].

The FUV light short of the Lyman edge ($\lambda = 912$ Å) ionizes neutral hydrogen.
As a result, most of this radiation is absorbed in the ISM or IGM and does not reach
our telescopes. Instead, a sharp drop, known as the Lyman break, appears in the FUV
spectrum. This property is conveniently used for determining the galaxy redshift at
various epochs of cosmic history (Sect. 4.1, Fig. 6). Part of the absorbed ionizing
radiation is reprocessed into emission lines which are formed by recombination and
which become another SF signature (Sects. 2.3 and 2.4). If, on the other hand, the
column densities of interstellar H I are low enough not to remove all of the Lyman
continuum, the remaining radiation will escape to the surrounding IGM and ionize
it—which is of great interest mainly to the high-z studies and the era of cosmic
reionization ($z > 6$, Sect. 5.2).

2.2 UV Absorption Lines

UV-bright galaxies allow observation of starburst properties through UV absorption
lines formed in the foreground ISM (Fig. 2). The lines are especially well detectable
in starbursts producing copious amounts of young stars and thus UV photons. The
lines inform us about chemical composition of the ISM gas and its ionization state
(e.g. Si II, Si III, Si IV), about kinematics and about optical depth of the gas. The
FUSE satellite opened the way to studying the UV lines in the MW and nearby
galaxies, as it was the first UV facility with sufficient spectral resolution. The *HST*
has then revolutionized the field with progressively more sensitive spectrographs
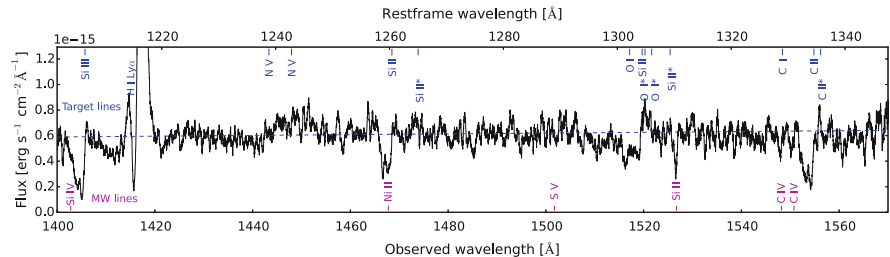
Fig. 2 UV absorption lines of the galaxy SDSS-J030321.41-075923.2. The major lines originating
both in the galaxy and in the Milky Way have been labeled. Source: *HST* archive

and improving resolution: GHRS, STIS, COS. Conversely, at high redshift, UV lines are reachable with ground-based optical telescopes, which need to have a sufficient collecting area and a spectrograph of sufficient resolution.

The UV absorption lines probe gas kinematics in nearby starbursts, showing that their properties may range from static to high-velocity ($\sim$1000 km s^{-1}) outflows [19, 20], and may vary between different gas phases. Outflows were also found to be ubiquitous at high redshift [21]. The UV absorption lines thus offer useful tools for answering questions about stellar feedback, ISM enrichment, IGM enrichment, gas flows, and galaxy evolution. We describe in Sect. 2.3 that the UV lines also represent valuable complementary information for interpreting the Lyman-alpha line. Eventually, the optical depth of the UV lines has been explored as a tool for studying the escape of ionizing UV continuum from galaxies [19]. If the neutral gas situated along the line of sight does not completely cover the ionizing source, we should observe residual flux in the absorption lines. This can in turn be translated to the Lyman continuum escape fraction [22]. However, in reality, the interpretation of residual fluxes is not straightforward, is dependent on the gas geometry, its chemistry, on spectral resolution, and on the applied model. Observational testing of the method against the directly measured Lyman continuum escape has only started recently, after the first successful Lyman continuum detections have been confirmed [23, 24].

2.3 *Lyman-Alpha Line of Hydrogen (UV)*

Lyman-alpha (Lyα), at wavelength $\lambda = 1215.6$ Å, is the first transition of hydrogen and in principle its brightest spectral line. In galaxies, it is produced by the recombination process in the regions of ionized gas mostly around hot stars and AGN. The probability that the recombination cascade passes through the first transition is $\sim$70% and Lyα thus reprocesses a major part of the stellar ionizing radiation. It may hence appear as the ideal signature of star-forming galaxies and it was indeed predicted to be the beacon of high-z galaxies as early as the 1960s [25]. However, the reality is less straightforward: Lyα undergoes a complex radiative transfer in the neutral ISM of the galaxy and the IGM. By symmetry, its cross-section for interaction with neutral hydrogen is large and the line becomes optically thick at H I column densities as low as 10^{13} cm^{-2}, i.e. basically in all galaxies (see a useful review of Lyα physics by M. Dijkstra [26]). Observational confirmation of Lyα only came almost 20 years after the prediction and the line was far weaker than expected ([27] in low redshift; [28] in $z \sim 3$; first *HST* Lyα images in [29]).

The Lyα physics started to emerge with the growing observational samples both at low and high redshift, and, in parallel, with the development of numerical models. Building on analytical solutions that were only possible for a few extreme cases [30], the numerical codes explore a range of geometries and conditions, from homogeneous spherical set-ups [31, 32], through clumpy media [33] to full hydrodynamic simulations [34]. The resonant scattering off hydrogen atoms
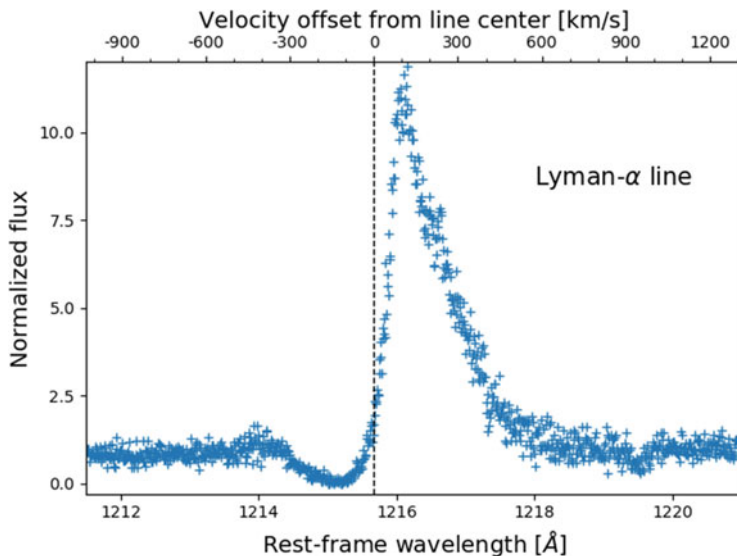
Fig. 3 Lyα spectrum of Mrk 259, a nearby irregular starburst galaxy from the LARS sample. The P-Cygni profile with its asymmetric red peak and the absorption trough blueward from the line center (1215.67 Å, dashed vertical line) result from radiative transfer. Credit: *HST* archive

increases the probability of Lyα destruction by dust, therefore the dust role is enhanced with respect to other UV wavelengths. The Lyα line is further sensitive to the geometry of the medium, its clumpiness, and the macroscopic and microscopic kinematics. To escape from the ISM, the Lyα photons must either shift to regions where the H I density is low, or shift in frequency to the line wings (by interaction with hydrogen atoms) where the scattering cross-section is smaller. As a result, Lyα galaxy images commonly show a "halo", which here means a low surface brightness Lyα emission extending beyond the stellar continuum image [35–37]. This feature is likely due to photons produced in the starburst regions and transferred to the outskirts of the galaxy. Conversely, the Lyα escape through a frequency shift is detected in spectral line profiles, which range from asymmetric P-Cygni (absorption in the blue, emission in the red, see Fig. 3), through single red peaks (mostly in high z), double- or multiple-peaks, to damped absorption profiles (with no escaping photons). All of the profiles result from radiative transfer of photons from the line core to the line wings.

Despite its complex interpretation, Lyα is one of the primary tools for galaxy detection at high redshift (Sect. 4.2). Now that we are aware of its limitations and we search in the correct luminosity range (much fainter than the theoretical one), Lyα stays detectable out to redshifts beyond $z \sim 10$. As demonstrated in the local universe (from the earliest studies such as [27, 38]), the Lyα emission is only present in a subset of star-forming galaxies and therefore introduces selection biases that may not be fully understood today. Lyα is mostly bright at low-mass, low-

metallicity, dust-poor starburst galaxies (not speaking about quasars here). However, due to the multi-parameter nature of Lyα transfer, we do not have a full control of the galaxy populations detected in Lyα, and complementary methods are necessary for characterizing galaxy evolution at high redshift. A good lesson was provided by the extremely low-metallicity, dust-poor local galaxy IZw18, where bright Lyα emission was expected and where the *HST* revealed a deep absorption instead [39]. We understand now from the UV metal lines that the neutral gas is static in IZw18, which disables the Lyα escape. We have to take into account these effects when interpreting high-z samples, especially in experiments where only emission is targeted.

At present, Lyα imaging and spectroscopy are among the main objectives of all currently developed facilities such as the James Webb Space Telescope (*JWST*) and the generation of extremely large telescopes (ELTs). The Subaru telescope has its powerful Hyper-Suprime Cam, the ESO's Very Large Telescope (VLT) recently obtained the highly performant integral-field spectrograph MUSE optimized for Lyα, and its successor HARMONI is in development for the ESO's ELT. The Hobby Eberly Dark Energy Experiment (HETDEX) is expected to detect millions of Lyα galaxies. Lyα will therefore stay a substantial cosmological tool in the years to come, despite all its limitations.

2.4 Optical Emission Lines

Starburst galaxies are characterized by bright optical emission lines that are formed in the ionized interstellar gas (see Fig. 5). Part of the lines arise from recombination, and represent thus reprocessed ionizing radiation of O and B stars. This is the case of the hydrogen Balmer series, for instance. The Hα line can reach equivalent widths over thousand Å in starburst galaxies. The Hα luminosity is also one of the favourite tools for SFR determination [1].

Forbidden lines represent another type of transitions, excited by collisions and de-excited radiatively. Their luminosities are not directly coupled to the ionizing luminosity, but they are bright in starburst galaxies thanks to the high temperatures and the energy pumped into the ISM by star formation. Forbidden lines of S^+, N^+, O^+, O^{++} are the most prominent ones. Their formation is sensitive to metallicity, electron temperature and density, therefore the ratios of the line fluxes are useful for measuring the fundamental gas properties. In addition, their combinations allow classifying the galaxies to AGN and star-forming galaxies. Statistical classification trends emerged from the pioneering work of Baldwin, Phillips and Terlevich (their so called BPT diagram [40]) and similar. Building on these early works, the big data brought about by the Sloan Digital Sky Survey (SDSS) at the turn of this century led to the discovery of a clear separation between star-forming galaxies and AGN into two narrow sequences in the BPT diagram [41]. Theoretical works such as [42–44] provided interpretation and prescription for the observational patterns. The oxygen [O III]λ5007 line is among the brightest optical lines under certain conditions.

Sensitive to the temperature, the line is bright in low-metallicity environments (around 10% solar, e.g. in dwarf starburst galaxies) and in high-excitation regions (in AGN). A second line, such as [N II] $\lambda6583$ in the BPT diagram, is necessary for discriminating between the low-metallicity starburst and the AGN. In extreme starbursts, such as those at high redshift, the division between SF and AGN becomes more delicate: the extreme ISM conditions produce emission line fluxes originally believed to exist only in AGN. Recent detections of powerful starbursts thus make us revise existing models and our understanding of star formation [44].

The optical band also hosts spectral lines that are related to specific astrophysical questions connected to the starburst. One of the examples is the lines produced by Wolf-Rayet (WR) stars, the evolved descendants of O stars. A blue bump around 4600 Å and a red bump around 5700 Å, both formed by a gathering of several emission lines, are characteristic WR features. He II lines such as 4686 Å can also be of WR origin. The WR evolution is strongly affected by metallicity: at low metallicities, only the most massive stars become Wolf-Rayet, probing thus the high-mass end of the initial mass function (IMF). For more details on WR observations, we refer to [45]. Another example is the use of optical lines for probing the primordial helium abundance. While the oxygen abundance (O/H) varies among galaxies, the helium abundance (Y) stays nearly constant. By extrapolating the measured trend to zero O/H, one should retrieve the primordial Y. Observations of low-metallicity star-forming dwarfs play a decisive role in this problem [45].

Detection of the brightest rest-frame optical lines (Hα, Hβ, [O III], [O II]) at high redshift has been achieved in the last decade using the 8–10 m telescopes such as the Very Large Telescope (VLT), the Keck Telescope or Subaru. Future larger samples and a more complete coverage of lines will provide important clues to the conditions in the distant galaxies.

2.5 Infrared Emission

Star formation takes place in dense molecular and dusty clouds. It has been approximated that dust absorbs half of the stellar light produced in the universe and re-emits it in the infrared. As the absorption is particularly efficient in the UV, the IR band is an important complement to the UV SFR estimators. The IR alone is not sufficient to correctly retrieve the SFR, but the combined UV and IR measurements proved to be an efficient method. The IR correction can be essentially negligible in dust-poor dwarf galaxies and metal-poor regions, but its importance increases with growing metallicity and dust content. On the other hand, the IR emission can significantly overestimate the SFR in the cases where evolved stars contribute to dust heating. The conversion factor between dust emission and SFR must therefore be a function of the stellar population [3].

The far-IR emission is from 99% composed of continuum radiation produced by dust grains. The remainder is line emission from atomic and molecular transitions in the ISM gas, concentrated in a small, sub-kpc region. The IR continuum depends on

the dust content and composition, but also on the spectrum of the starlight: luminous young stars will heat dust to higher temperatures than old stars and their thermal IR will thus peak at shorter wavelengths ($\lesssim 60\,\mu m$). The complexity of dust emission features corresponding to small and large dust grains at different temperatures have been summarized in excellent review papers by Calzetti [17] and Kennicutt [3], together with the IR SFR calibrators. For the purposes of this text, we only need the qualitative statement that the IR emission provides an important window for detecting obscured starbursts at both low and high redshift (Sects. 3.5 and 4.3).

2.6 X-rays

X-rays trace the star-forming activity through its final products—X-ray binaries—and through accompanying phenomena such as heating of the surrounding ISM by stellar feedback and supernovae. Binary systems composed of a main-sequence star and a compact object—black hole or neutron star—emit X-rays by accretion of matter, transferred from the donor star onto the compact object (see review [46]). The systems are classified as high-mass or low-mass X-ray binaries according to the mass of the donor star. Starbursts are characterized by prominent X-ray emission that is dominantly provided by the rapidly evolving high-mass X-ray binaries (HMXBs). Additional X-ray luminosity is provided by interstellar hot gas peaking at $\sim 1\,keV$ and a few additional sources such as low-mass X-ray binaries or cataclysmic variables. In addition, more exotic sources may contribute decisively: ultra-luminous X-ray sources (ULX) whose nature is debated (extreme X-ray binaries, anisotropic emission, neutron stars) [47], and intermediate-mass black holes (IMBH). Such objects seem to be more probable at low metallicity and at high SFR [48].

X-ray emission has been mapped in a number of local dwarf galaxies including the low-metallicity IZw18, SBS0335-052 [49], Haro 11 [50] and other starbursts [51–55]. Their X-ray luminosity is generally dominated by several extremely bright, point-like sources of debatable origin—usually too bright for "classical" X-ray binaries, they are suspected to be ULXs, IMBHs or even AGN (though often without optical counterparts). Empirically, the total X-ray luminosity of star-forming galaxies is proportional to the SFR [56] and inversely correlates with metallicity [53, 57, 58]. The theoretical basis for starburst X-ray emission was provided by numerical simulations of X-ray binaries and of hot gas emission [59–61]. X-ray observations remain challenging at high redshift, where they are restricted to images of stacked samples [53]. Together with sensitive, detailed, resolved mapping of nearby sources, the high-z observations will be a task for the new generation of X-ray satellites.

3 Local Starburst Galaxies

We will focus on global starbursts, rather than individual starbursting regions of massive galaxies (such as the central region of M82, or 30 Doradus in the Large Magellanic Cloud—Fig. 1). The latter are frequent in the local universe, the former are rare. Global starbursts are interesting from the cosmological point of view, as they are traceable out to the earliest epochs of the universe, where they were bright and numerous. The focus on global starbursts here predefines the focus on dwarf galaxies and on extremely dusty IR galaxies.

While dwarfs constitute the most common galaxy type in the nearby universe (>70%), only a few percent of them are starbursting. They have attracted attention for many decades [62, 63]. Their subsets appeared under various names in the past, such as H II galaxies [64] or blue amorphous galaxies [65], reflecting the techniques of their discovery and the focus on a particular feature at a time. Some of the starbursting dwarf classes will therefore partially or totally overlap. Our intention here is to mention those that have been extensively studied in recent past with the motivation to search for analogies with high redshift.

3.1 Blue Compact Dwarf Galaxies

Blue galaxies, associated with the bright continuum of young stars, attracted attention since the 1960s. The colour selection alone resulted in a mixed bag of galaxy morphologies and luminosities. A subset that appeared barely resolved on optical plates of that time got the name blue compact galaxies (BCGs). It is still a heterogeneous class which some authors, with the presently improved knowledge, further sub-divide by compactness, luminosity or morphology. Not all of the BCGs would comply with all the definitions of a starburst. Their common properties are relatively small mass ($<10^9\,M_\odot$), low metallicity, bright optical emission lines, and sizes within a few kpc. Galaxies discovered later (for instance by emission lines) and having similar properties have been added to the class. The most centrally peaked ones ($<2\,kpc$) are referred to as blue compact dwarfs.

BCGs include some of the most metal-poor galaxies (e.g. IZw 18, see [66]). This led to the thinking that they formed only recently (which would have profound implications for galaxy formation). However, this was disproved by the discovery of older stellar populations (see review [45]). Instead, their star formation has been inefficient for most of the history, interleaved with time-limited bursts. BCGs are gas-rich ($\gtrsim$50% of mass is in gas) and dust-poor. Their morphologies range from H II-region-like (Pox 186) to irregular and clumpy (see Haro 11 in Fig. 4) to more symmetric ones. Their morphologies and velocity fields often bear signs of a recent interaction, despite the relative isolation of many of them [14, 15, 45]. The presence of low surface brightness neighbours cannot be excluded in such cases. Interaction with neighbours may, in turn, be responsible for the starburst activity in BCGs. This

Fig. 4 A multi-color *HST* image of Haro 11, one of the nearest BCGs (and Lyman break analogues). Its irregular structure, of total diameter $\sim$2 kpc, is probably the result of a galaxy merger, which also induced the SFR $\sim$20 $M_\odot$ year^{-1}. The galaxy is a weak Lyman continuum leaker (Sect. 5.2). It is a Lyα emitter in some of the star-forming knots and a Lyα absorber elsewhere. Credit: ESO/ESA/Hubble and NASA (https://www.eso.org/public/images/)

comes with a limitation that it is uncertain if interaction of two dwarfs is sufficient for triggering SF as in massive galaxies—in dwarfs, the gravitational effects are equally strong as the turbulent velocities caused by stellar winds. Starbursts in BCGs challenge the models of star formation anyhow: dwarfs are generally inefficient in converting gas to stars due to the weak gravitational bounding. In addition, the existence of molecular gas in BCGs is difficult to prove due to their low metallicity. Nevertheless, starbursts in BCGs do exist.

There have been long-standing debates about the evolutionary relation between BCGs and other dwarf galaxy classes [14]. Answering these questions is obviously interesting with respect to the high-z universe, where galaxies of similar masses were prevailing. For the same reason, BCG observations in the UV and Lyα are important. For their low dust amount, a bright Lyα emission was naively expected in all BCGs. This hypothesis was disproved by observing a similar incidence of emission and absorption Lyα profiles [38]. The extremely metal-poor IZw 18 is one of the surprising examples of a deep absorption. This finding illustrates the importance of H I kinematics for the Lyα escape [67], which we described in Sect. 2.3. The absence of Lyα emission in a subset of BCGs is an important realization for high-z surveys, where the Lyα technique will certainly be missing such galaxy populations.

3.2 Lyman-Alpha Reference Sample

Efforts to understand high-redshift galaxies have led to a definition of the local Lyman-alpha reference sample (LARS) [68]. The Lyα line becoming one of the dominant tools for galaxy detection at high redshift, the need was to understand the mechanisms of its formation and transfer through the ISM. This is achievable in the local universe, where spatial resolution and multi-wavelength data are available.

The LARS sample targeted star-forming galaxies (requiring Hα equivalent widths above 100 Å) with FUV continuum luminosities similar to the $z \sim 3$ LAEs and LBGs. The sample comprises over forty galaxies at redshifts $z = 0.03$–0.2, observed with multiple *HST* broad-band and narrow-band filters, complemented with *HST* COS spectra, and ground-based data including optical integral-field spectroscopy and H I radio interferometry. To obtain *HST* Lyα images [35], a dedicated method of broad-band filter subtraction was developed, due to the lack of existing appropriate narrow-band Lyα filters.

The UV-based selection produced a sample composed of irregular galaxies bearing signs of interactions, and disk/spiral galaxies. Their Lyα shows a variety of properties, from absorption to bright emission, including extended diffuse Lyα halos that reach beyond the stellar or Hα emission [35]. The high-resolution images comparing the stellar light, the optical gas emission and Lyα thus show how Lyα travels from the productions sites (which should be identical to Hα) to regions where it can easier escape. In complement, the UV and optical spectroscopy probe the effects of gas kinematics on the Lyα escape [69, 70], while the radio 21cm data demonstrate the importance of the H I mass [71]. Such detailed observations are by far not available for high-z galaxies, and therefore LARS, as its name indicates, provides a local reference sample for aiding the interpretation of high-z observations.

3.3 Lyman-Break Analogues

As soon as the Lyman-break technique proved efficient for detecting galaxies at high redshift (Sect. 4.1), the question arose what type of galaxies were selected by this approach, especially in the situation where the FUV was the only available signal. The rest-frame UV properties were better mapped in high redshift than locally, and therefore it was impossible to draw analogies with nearby galaxies. Launch of the GALEX mission remedied this situation in the early 2000s and finally enabled the construction of statistical samples of low-z UV galaxies.

Lyman-break analogues (LBAs; formerly called UV-luminous galaxies, UVLGs) were selected from the GALEX archive as galaxies at $z < 0.2$ with FUV luminosities similar to those observed by the Lyman-break technique at high redshift [72]. Such galaxies are rare in the local universe; the FUV selection resulted in $\sim$70 targets. The GALEX and SDSS images reveal that their morphologies range from compact systems with radii of 1 kpc to large, late-type, 10 kpc-size and 10^{11} $M_{\odot}$ mass galaxies. The compact targets share many properties with the high-z samples: they have stellar masses of $\sim 10^{9.5-10.7}$ $M_{\odot}$, SFR $\sim$5–25 $M_{\odot}$ year^{-1}, and metallicities 12+log(O/H)$\sim$8.2–8.7. Lyman-break galaxies at high z, on the other hand, can reach significantly higher SFRs (few hundred $M_{\odot}$ year^{-1}) and they span a significantly larger metallicity range (12+log(O/H)$\sim 7.7 - 8.8$). Also, the local LBAs do not reach the maximum FUV luminosities of high-z targets, the overlap between the FUV luminosities is achieved only close to the lower edge of the high-z FUV luminosity interval.

Today, spectra and images at several wave bands are available for a subset of LBAs, including optical and UV data obtained with the *HST*, and X-ray data from *Chandra*. Thirty percent of the large LBAs and 15% of the compact LBAs were found to be type-2 AGN [72] (while type-1 AGN were removed from the sample upon selection). Among the star-forming LBAs, a subset have been studied in more detail, revealing starburst character of their spectra, including strong optical emission lines, emission in the Lyα line [19], and in X-rays [58, 73]. Their X-ray emission is among the brightest detected so far, with luminosity similar to high-redshift Lyman-break galaxies, and with resolved ULX sources or AGN candidates. LBAs are also possible Lyman continuum leakers thanks to their fast stellar winds [19]. The Lyman continuum escape has indeed been confirmed for several LBAs [74].

3.4 Green Peas and Luminous Compact Galaxies

Green Peas were identified in the SDSS by the citizen science Galaxy Zoo project [75]. The targets that appear green and point-like, i.e. unresolved by the SDSS, turned out to be compact, highly star-forming galaxies at redshift $z \sim 0.2$. Their green colour is caused by bright optical emission lines. In particular, the [O III] λ5007 line reaches equivalent widths above 1000 Å (Fig. 5). It was shown later that the original eighty Green Peas are part of a more general population extending over a large interval of redshifts (at least $z \sim 0.02 - 0.6$, probed by the SDSS), while they change colour accordingly with the emission line shift to other filters. More than 800 such objects were identified in the SDSS and were named Luminous Compact Galaxies in [76].

GP stellar masses are in the range 10^8–10^{10} $M_{\odot}$, their SFR $\sim 1 - 60$ $M_{\odot}$ year^{-1}, and oxygen abundances $12 + \log(O/H) \sim 8.05$–8.15 [76]. For those where UV data are available ($\sim$40 targets [77–80]), the Lyα line is observed in emission and many of the GPs would pass the selection criteria of high-z Lyman-alpha emitters
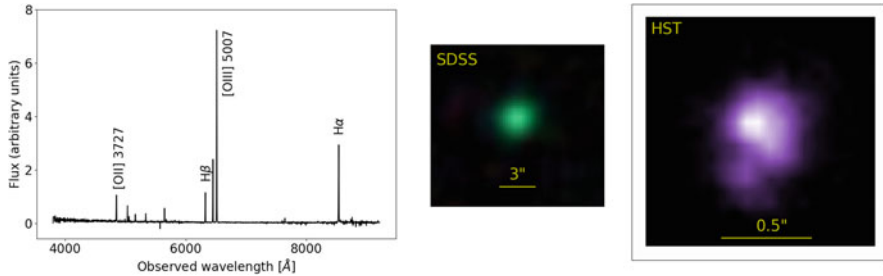
Fig. 5 Green Pea optical SDSS spectrum (left); optical SDSS image—unresolved (middle); and near-UV *HST* image—obtained for Cosmic Spectrograph spectral acquisition (right). All three panels are for the galaxy SDSS J092532.36+140313.0 at $z \sim 0.3$. The diameter $0.5''$ corresponds to ~ 2 kpc. Credit: SDSS and *HST* archives

(see Sect. 4.2). Their resolved *HST* images typically show a knotty structure (Fig. 5). Some of targets appear compact and structureless even with the *HST* resolution [81], which can however be a question of data depth.

Do the Peas represent a new class or are they related to the other dwarf populations, such as the BCGs? An evolutionary link is improbable, as the average GP masses and metallicities are larger (at an earlier cosmic time) than those of the average BCG. The continuity of the dwarf populations across redshifts is still being debated. Nevertheless, both GPs and BCGs represent the rare types of nearby dwarf starburst galaxies that are more typical of high-z universe, with low masses and metallicities, irregular morphologies, and low dust amounts. In contrast, there is a clear overlap between Green Peas and LBAs. While LBAs were UV-selected, the GPs were identified in the optical, but their follow-up UV observations show that they are conform with the LBA selection criteria.

Green Peas (or Luminous Compact Galaxies) were among the first targets where a large escape of ionizing UV continuum was discovered [81, 82], as we describe in Sect. 5.2. This strengthens their role of local laboratories for the reionization era galaxies ($z > 6$). GPs are bright in X-rays [55], consistently with their high SFR and low metallicity. They are among the brightest star-forming galaxies known to date, exceeding the empirical calibrations such as [56, 58]. This implies the presence of powerful X-ray sources, most likely the end products of massive stars, or potentially low-mass AGN [83]. Nevertheless, this X-ray enhancement is not present in all GPs, some are X-ray sub-luminous [55]. This diversity in X-ray properties probably requires the dominance of extreme, short-lived sources such as ULXs.

3.5 *Dusty, Luminous Infrared Galaxies (LIRGs)*

Galaxies with large amounts of dust are invisible or exceptionally faint in the UV and optical. Instead, their bolometric luminosities are dominated by the dust-

reprocessed IR radiation. Galaxies bright in the far-IR wavelengths were first reported in the 1960s, but dramatic progress was achieved with the IR satellites—*IRAS* in the 1980s, Spitzer, Herschel and WISE after the year 2000—and the ground-based SCUBA array. The most luminous targets were classified (somewhat arbitrarily) into Luminous Infrared Galaxies (LIRGs) for luminosity $L_{IR} \geq 10^{11}\,L_\odot$, and Ultra-luminous Infrared Galaxies (ULIRGs) for $L_{IR} \geq 10^{12}\,L_\odot$. The dusty infrared galaxies are fascinating objects with colossal star-formation rates reaching $1000\,M_\odot\,year^{-1}$, which are among the largest known. Such a vigorous SF is necessarily short-lived because of the finite gas supply. The (U)LIRG may therefore represent an evolutionary phase, possibly coming after a violent event such as a gas-rich galaxy merger. The merger would trigger the SF, which is subsequently responsible for the dust and for the obscured (U)LIRG. The obscured phase can possibly become an optically luminous AGN by blowing away the dust. This scheme is still a matter of a lively debate, with uncertainties about its universality between different galaxy types, different redshifts and different environments. The literature about (U)LIRGs is vast, the puzzle of their origin and future as well. We here describe the basic properties and we refer to the detailed reviews provided by Blain et al. [84], Lonsdale et al. [85], and Casey et al. [86], which contain a plethora of additional papers to read.

LIRGs and ULIRGs are massive galaxies, their morphologies include ellipticals, lenticulars, and spirals. Their dust temperatures vary between different targets, may vary with redshift, and multiple dust components are often present in the same galaxy (mostly ranging from 20 to 100 K). It is interesting to note that Lyα emission has been observed in some (U)LIRGs despite the large amounts of dust [87]. Gas kinematics play a decisive role for the Lyα escape there—high-velocity outflows ($900\,km\,s^{-1}$) were measured, using the UV absorption lines of metals. To account for the large IR luminosity, (U)LIRGs necessarily host a powerful UV source: an AGN, a starburst, or both. Optical studies have found AGN-like spectral lines in $>30\%$ ULIRGs, in parallel with evidence for a strong star formation in all targets. The incidence of AGN possibly increases with luminosity, some studies claim the AGN presence in more-or-less all ULIRGs. The difficulty of AGN confirmation lies in the ULIRG massive obscuration that makes even the X-ray detection uncertain. ULIRGs were originally claimed sub-luminous in X-rays, but sensitive observations and polarized light observations discovered previously unknown active nuclei. Some of the ULIRGs host two or more AGN, and thus provide direct evidence of galaxy mergers. Deep optical and NIR imaging demonstrated that a vast majority of ULIRGs are located in interacting systems, ranging from widely separated galaxies to advanced mergers. Evidence of interaction between more than two galaxies led to the hypothesis that ULIRGs trace the previous presence of compact galaxy groups. Nevertheless, they never reside in rich environments such as galaxy clusters.

The causal relation between (U)LIRGs and quasars remains an open question that is being studied across redshifts by evaluating the clustering properties of both populations as well as their internal structure. One hypothesis is that (U)LIRGs are obscured quasars seen edge-on, and can thus be part of the AGN unification scheme. A prevailing theory is the evolution of (U)LIRGs into unobscured quasars

and then into elliptical galaxies [11, 85]. ULIRGs represent only <0.1% galaxies in the local universe, but were much more common in the past, with a distribution peak at redshifts $z = 1$–3. High redshift holds the key to understanding these galaxy populations that we will discuss more in Sect. 4.3.

4 Starburst Galaxies at High Redshift

Starburst was a popular mode of star formation in the early universe, unlike today where it is much rarer. High-z starbursts formed a large fraction of today's stars and most probably provided the building blocks for galaxies as we know them today.

The knowledge attained to date about high-z galaxies is less complete than that about the local universe. Until the 1990s, only AGN were observable at redshift $z > 1$ (i.e. universe younger than 7 Gyr). Since then, technological progress in telescopes and detectors has allowed probing galaxy populations out to $z \sim 10$ (i.e. 500 Myr after the Big Bang). Still, their low surface brightness and the small angular size only allow detection of their brightest features, mostly without angular resolution. It is therefore convenient to design observational methods so as to target the prominent starburst signatures that we described in Sect. 2. Essentially all galaxies detected so far at high z are hence starbursts and the galaxies are classified by the detection method, instead of morphology or other physical properties. The samples of brightest high-z galaxies are complemented with lensed galaxies, which provide more detailed, deeper and spatially resolved information, reaching surface brightness much fainter than would be detectable without the gravitational lens.

4.1 Lyman-Break Galaxies

The Lyman break imaging method uses the fact that starbursts are UV-bright, with a sharp drop at the edge of the Lyman sequence, i.e. $\lambda < 912$ Å (Sect. 2.1). The Lyman break is conveniently shifted to optical wavelengths at $z > 2.5$, and to NIR at $z > 7$, reachable by ground-based telescopes. The sky is imaged in a set of optical and NIR filters that sample the galaxy spectral energy distribution (SED). Cross-correlation of the sky maps in different filters will show galaxies that are detected in longer wavelengths and undetected in bluer filters. The disappearance of a galaxy from the filters corresponds to its Lyman break. The dropout filter provides its approximate redshift, with precision $\delta z \sim 0.1 - 0.2$ (Fig. 6). Objects detected by this technique are referred to as Lyman-break galaxies (LBGs) or dropout galaxies. The advantage of the method is the use of broad-band filters, and thus an efficient retrieval of large galaxy samples. The precise redshifts are then secured with follow-up spectroscopy that requires significantly longer exposure times. As we approach the reionization era, the Lyα forest becomes so optically thick that it removes essentially all the flux at $\lambda < 1216$ Å (Sect. 5.1), and therefore the Lyman break technique actually
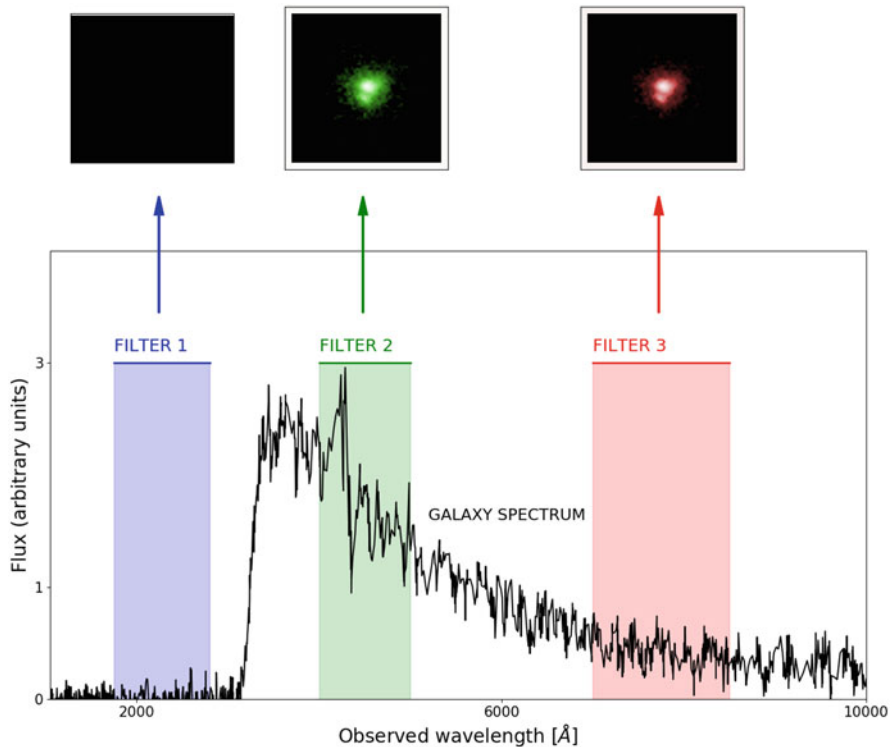
Fig. 6 LBG detection technique: (mock) galaxy is detected in a set of filters (here green and red), while no detection is achieved in the blue filter. The blue filter thus corresponds to wavelengths shorter than the Lyman break. A typical galaxy spectrum (rest-frame UV) is shown with the black line, here at redshift $z = 2.5$

becomes the Gunn-Peterson trough technique, detecting the sharp drop blueward of Lyα.

After the pioneering steps in the LBG technique, breakthrough discoveries were done by Steidel et al. [88] at $z \sim 3$. They started with 4-m telescopes such as the William Herschel Telescope in 1993 and then switched to the 10-m Keck Telescope and to the Hubble Space Telescope (Hubble Deep Field survey). Nowadays, the known LBG samples count tens of thousands of targets, 90% percent of which are situated in the redshift interval $z \sim 2.5 - 3.5$. Observations at $z > 5$ became possible later, with the development of more sensitive instruments, which was especially true for $z > 7$, where the Lyman break shifts to the NIR. The Hubble Deep Field, Hubble Ultra-Deep Field, and the GOODS survey have been prolific at identifying LBG populations out to redshifts $z = 7$–10 [89]. In addition, galaxies detected through the Lyα line (Sect. 2.3) may form a subset of the LBGs and provide thus complementary information.

The typical LBGs have stellar masses ranging from 10^9 to $10^{11}\,M_\odot$, and metallicities from 10% solar to solar. More detailed information is available for a few LBGs that are in fortuitous alignment with a foreground galaxy and are thus gravitationally lensed: e.g. the Cosmic Horseshoe [90], the Cosmic Eye [91], the 8 o'clock arc [92], or the Sunburst Arc [93]. The lensing provides clues about their geometry, ISM composition and kinematics, about stellar populations, and about the escape of ionizing radiation. Most of the lensed LBGs seem to be rotating disk galaxies with multiple giant star-forming H II regions that have a SFR density two orders higher than spiral galaxies seen in the local universe. The comoving number density of LBGs is similar to present-day bright early-type galaxies, and therefore an evolutionary link between the two is possible. However, whether their evolution proceeded through major mergers, or they are cores of present-day galaxies which evolved passively without major events, still needs to be clarified. To this end, deep multi-wavelength spectroscopic follow-ups are necessary (and challenging) in order to constrain the morphologies, precise masses, velocity fields, duration of the star-forming activity, and evolution of LBGs across redshifts. Useful review papers were provided by Giavalisco [94] and Dunlop [95].

4.2 Lyman-Alpha Emitters (LAEs)

Lyman-alpha emitting galaxies were important constituents of the high-z universe, as they represent the majority of the known star-forming galaxies at redshifts close to reionization. Using Lyα as a detection tool was proposed as early as the 1960s [25]. However, the first Lyα detections were not available until the 1980s [28] when sizes and sensitivities of telescopes and detectors became sufficient. The Lyα fluxes were several factors lower than expected, as we explained in Sect. 2.3. Still today, predicting the Lyα luminosity for an individual galaxy is not straightforward due to the multi-parameter nature of the Lyα escape. The largest ground-based telescopes and space telescopes (*HST* and soon *JWST*) are used for observing high-z LAEs today. The asymmetric Lyα spectral profile (Sect. 2.3, Fig. 3) presents an advantage for high-z surveys, where it allows a unique identification of the line and hence of the galaxy redshift. Recently, LAE surveys have gained another dimension thanks to the use of integral-field spectrographs such as MUSE at the ESO VLT [37]. Simultaneous observation of spectra from different parts of the galaxy allows testing the theories of Lyα transfer from the production sites all the way to the outskirts.

Narrow-band Lyα imaging surveys pick galaxies where Lyα is produced in large quantities and is only weakly attenuated. This requires a powerful starburst activity together with low amounts of dust and neutral hydrogen, as well as the presence of outflows that shift Lyα out of resonance. These conditions are met in low-mass galaxies (typically 10^8–$10^{10}\,M_\odot$), but not only. The low stellar mass facilitates the action of stellar feedback that can more easily outweigh the gravitational potential. However, the conditions that allow Lyα to escape span a certain range (Sect. 2.3),

and therefore the possible LAE masses and dust amounts can be larger in special cases. The escape of Lyα photons may also be non-isotropic due to the disk galaxy morphology [34], due to gas clumpiness or preferential directions of escape [96, 97]. To improve our understanding of what galaxy population is selected by Lyα, several studies have searched for the differences between LAEs and the continuum-selected LBG or the emission-line-selected (in the sense of rest-frame optical) galaxies on the same redshifts. No statistical differences were found between LAEs and optical emission-line galaxies in the morphology, inclination, sSFR, UV slope or the distance between neighbours [98], suggesting that the Lyα escape is driven by the detailed local physics rather than by global properties. Some LBGs are bright in Lyα, therefore the LBG and LAE populations at least partially overlap. The mean LAE mass is usually found to be one or two orders of magnitude lower than the mean LBG mass. However, there are studies that claim no differences between the two populations (discussed in [98]). On the other hand, clustering properties of LAEs and LBGs seem to differ, suggesting their different evolutionary paths [95, 99].

The fraction of Lyα photons that escape from galaxies evolves with redshift [100]: the average escape fraction increases from $z = 0$ to $z = 6$ and declines at $z > 6.5$. The increase correlates with a decreasing dust amount in the cosmos, suggesting that dust could be the main driver of the *average* Lyα escape (modulated by other parameters [101]). The escape fraction drop at $z > 6.5$ can be attributed to the progressively more neutral IGM i.e. an effect of the environment rather than the galaxies themselves. The drop may also be an intrinsic feature of the reionization era galaxies, either due to a large fraction of static H I (as in the local IZw18) or the opposite, the Lyman continuum escape. At redshift $z > 6$, not only the escape fraction, but also the number of observed LAEs decreases, either due their intrinsically lower numbers or due to the neutral IGM. LAEs are currently observed out to redshifts $z > 10$, and play thus an important role as cosmological tools [99, 102–104]. Clustering properties map the dark matter structures and the evolution of LAEs through redshifts to the present day. The clustering suggests that they were the building blocks of the present-day MW-type galaxies [105]. The LAE clustering in the reionization era probably also maps the patchy IGM ionization. The importance of LAEs is reflected in the objectives of the new generation of telescopes, such as the *JWST* or the ELTs, with the ambition to use Lyα to detect the first galaxies in the universe.

4.3 Sub-millimeter Galaxies

High-redshift counterparts of local ULIRGs, i.e. dust-obscured, massive starbursts (Sect. 3.5), are known under the name Sub-millimeter galaxies (SMGs). Their detection has been effectively possible since the operation of the SCUBA bolometer array on Mauna Kea in the 1990s (see review [84]). Nowadays, several sensitive mm/sub-mm telescopes are available, including IRAM (Spain), NOEMA (France),

or ALMA (Chile). To facilitate the orientation in the vast literature on the subject, we refer preferentially to review papers in this text.

Typically scaled-up versions of ULIRGs, the SMGs are the most intense SF sites and the most bolometrically luminous galaxies in the universe ($L_{bol} \sim 10^{13} \, L_{\odot}$). Their molecular gas masses reach $10^{11} M_{\odot}$ and they fuel star-formation rates exceeding $1000 \, M_{\odot} \, year^{-1}$. ULIRGs were once thought to be evolved versions of SMGs. However, today's view is that SMGs were more massive and cooler than ULIRGs and thus any evolutionary link between them is unlikely. While the number density of nearby ULIRGs is one per four square degrees, there were hundreds per one square degree at $z > 1$ [85]. Cosmologically, SMGs should be the tracers of massive dark matter halos and their evolution across cosmic history. Recent instrumental advances (especially ALMA) have permitted the first studies of SMG clustering properties (reviewed in [86]), which will allow testing the theories of the SMG origin and their fate. High-z SMGs were predicted to reside in rich environments where they would accumulate their mass. According to today's knowledge, SMGs mostly appear to live in relative isolation (contrary to the predictions), even though they bear signs of galaxy mergers. Only the most luminous SMGs have been identified to reside in potential proto-clusters of galaxies [86].

SMGs show a surprisingly diverse range of optical properties, from undetected to bright sources. The optical spectra provide evidence for both starburst and AGN, residing in metal-rich gas. The bolometric luminosity is typically dominated by star formation. The lower limit for AGN incidence in SMGs is 30%, though in reality is probably significantly larger. The incidence seems to increase with luminosity and therefore with redshift. Intriguing results have been provided by radio observations showing that ∼70% of SMGs are spatially extended on ∼10 kpc scales, i.e. dramatically larger than the dust emission that tends to be concentrated in <1 kpc. Several interpretations of the radio emission exist, ranging from large-scale SF to jet-like structures similar to those in radio AGN [85]. SMGs are also known as sites of gamma-ray bursts (GRBs), ignited at the death of massive stars.

The present-day mainstream hypothesis is that SMGs evolved into quasars and eventually into early-type galaxies (nicely depicted in [11]). The SMG masses and SFRs indeed make them the ideal progenitors of elliptical galaxies. The existence of large numbers of massive galaxies such as SMGs out to high redshift represents a challenge to the simple hierarchical galaxy formation paradigm that predicted slow mass buildup through small galaxy mergers. On the other hand, it is not in contradiction with dark matter halo growth, which allows for rapid baryon accumulation in very massive halos [85]. The SMGs, their place in galaxy evolution, their progenitors and their successors thus play an important role in answering fundamental astrophysical questions such as the buildup of stellar mass in the universe, the origin of present-day galaxies, and the growth of supermassive black holes.

5 Role of Starburst Galaxies in Reionizing the Universe

5.1 Cosmic Reionization

The present-day intergalactic medium is essentially fully ionized, but it was not so during all of the cosmic history. After the early evolutionary stages where matter and radiation were constantly interacting, the universe became cool enough for radiation to split from matter at $z \sim 1000$ (i.e. $\sim$300,000 years after the Big Bang). The radiation then freely travelled through the universe without being absorbed by atoms. This was the start of Dark Ages, where the universe was neutral and without sources of radiation (apart from the H I line at 21 cm). The first stars are supposed to have formed at $z \sim 30$. Current observations have not yet reached such distant redshifts to capture their light. Nevertheless, an exceptional result was recently achieved: an absorption feature was observed in the H I 21 cm line profile, consistent with theoretical predictions of the effect of the first stars [106]. The observation thus proved that stars had been formed by $z \sim 20$. The phenomenon will further be explored by upcoming surveys such as LOFAR, HERA or SKA.

The birth of the first sources of light caused a phase change in the IGM: the IGM progressively evolved from neutral to a fully ionized state. The era between the appearance of the first stars and the redshift $z \sim 6$ where the IGM became essentially completely ionized is called the Cosmic Reionization. The end of reionization is well demonstrated by the Gunn-Peterson effect in quasars [107]: the FUV light of a distant quasar (or another bright source) encounters hydrogen clouds along the line of sight and the H I scatters away the light that gets in resonance with Lyα at the cloud's redshift. At different redshifts, different parts of the spectrum "become" Lyα, and, as a result, the original spectrum adopts numerous absorption features, known as the "Lyα forest". At $z > 6$, the discrete features turn into a continuous Gunn-Peterson trough that removes all the FUV at wavelengths shorter than the quasar's rest-frame Lyα [108]. Additional constraints for reionization come from the cosmic microwave background radiation measured with the *WMAP* and Planck satellites [109, 110].

5.2 Sources of Reionization: Starburst Galaxies?

Details of the cosmic reionization process depend on the density and distribution of gas, and, most importantly, on the available ionization sources, their density, distribution, evolution and energy spectrum (see review [111]). The first galaxies provided ionizing FUV radiation from hot, massive stars, and are thus natural candidates for reionization. Furthermore, quasars set in at some point, providing copious amounts of energetic radiation. Additional sources such as X-ray binaries or cosmic rays are being considered as possible ionization contributors (see references in [55]).

The distribution of the first galaxies was associated with dark matter structures, which are possible to model using cosmological simulations. Their ionizing photon production rate depends on the nature of the first stars and on the star formation rate density, for both of which we need an observational input in order to achieve realistic predictions [111]. However, yet another parameter controls the ionizing radiation (Lyman continuum) flux to the IGM: its escape fraction, reflecting the galaxy's ISM structure (total H I amount, dust, asymmetry, clumpiness). Numerical simulations predict that despite a strong variability of the escape fraction in time and in angular direction, an average value of ∼20% per galaxy is necessary to achieve the reionization solely by star-forming galaxies [112]. On the observational side, direct detection of the Lyman continuum from the reionization era galaxies is unfeasible: any ionizing photon that escapes from the galaxy will be absorbed by the neutral IGM and will not reach our telescopes. Only indirect signatures can be explored at the reionization era, while direct studies of the Lyman continuum leakage are restricted to lower redshifts, in practice $z \lesssim 3$, where the IGM H I amount is sufficiently low.

Searches for escaping Lyman continuum at any redshift were fruitless during two decades of observational efforts, except for a few sources with low leakage fractions [74, 113]. The situation has dramatically changed in the past few years. In 2016–2019, Lyman continuum was spectroscopically confirmed in approximately fourty $z \sim 3$ galaxies [114–118]. In parallel, a significant leakage was detected with the *HST* in eleven starburst galaxies of Green-Pea type at $z \sim 0.3$ (summarized in [81]). The Lyman continuum escape fraction reaches 70% in some of these targets, while their mean is ∼20%. Interestingly, this percentage is consistent with the numerical predictions mentioned above. Despite their too low redshift, the leaking galaxies support the possibility of cosmic reionization by their $z > 6$ analogues.

The low-z samples serve as laboratories for understanding the physical conditions that lead to a low optical depth at Lyman continuum wavelengths. From the current observations, we may speculate about the role of the galaxy compactness and low mass, which favour the escape of ISM gas from a shallow potential well and thus decrease the H I column. Second, low metallicity modifies stellar evolution, leading to a larger production of ionizing photons. Third, feedback from starburst-related processes (stellar winds, energetic photons and jets/outflows from compact binary systems) deposits radiative and mechanical energy into the ISM, which results in gas ionization and/or its removal along certain paths. Indirect indicators are being explored that would help us preselecting galaxies with Lyman continuum escape: various works probe the ISM ionization [119, 120], ISM velocities [19], saturation of the ISM spectral lines [121], X-ray emission [55], and the Lyα line profile [97, 122]. So far, the Lyα line was proven, both theoretically and observationally, to be the best indicator of the Lyman continuum escape, thanks to its sensitivity to the ISM properties [81, 97, 122].

A natural question is whether quasars, efficient producers of ionizing photons, could be the true sources of cosmic reionization instead of the star-forming galaxies. The question remains open so far. The first quasars formed in the reionization era, but it seems that they were not abundant enough at $z > 6$ to dominate the

reionization. However, with the scarcity of data, any new detection may change the picture [123–125]. Nevertheless, the Lyman continuum of starburst galaxies appears to be the most viable mechanism for reionization, winning over quasars or any other sources.

6 Conclusions and Future Prospects

It has been estimated in the literature that equal amounts of stars in the universe were formed in the following four types of environments: optically visible regions, dust-enshrouded regions of optical galaxies, heavily obscured galaxies with $L_{IR} <$ $10^{12} L_\odot$, and ULIRGs with $L_{IR} > 10^{12} L_\odot$ [126]. Dwarf galaxies dominated the star formation among the optically visible ones, while massive starburst galaxies are dusty and IR-bright. We have reviewed the different types of starburst galaxies both at low and high redshift. Without being complete, this overview illustrated the various possible manifestations of vigorous star formation, the corresponding detection techniques, the properties of various starburst galaxy populations, and their role in cosmic evolution. We demonstrated the search for analogies between low and high-redshift galaxies. Analogies allow complementary views on star formation and galaxy evolution, and on the origin and the future of starburst galaxy populations. In light of the analogies with high redshift, local galaxies have seen an increased interest in their classification by parameters such as the SFR, metallicity, FUV luminosity or compactness. While the overlap between high-z and low-z galaxy parameters cannot be perfect, the nearby galaxies serve as local laboratories that provide essential clues for the interpretation of processes in the distant universe where the details are unattainable.

Research on starburst galaxies has good prospects for future, and in particular galaxies at the cosmic dawn are among the main drivers for the new generation of astronomical instruments. MUSE, a sensitive optical integral-field spectrograph is already operating at ESO VLT. Its ability to simultaneously obtain hundreds of spectra per galaxy combines the advantages of classical imaging and spectroscopy. In combination with adaptive optics, MUSE reaches an angular resolution comparable to that of the *HST* and it can outperform the *HST* in detecting distant galaxies [127, 128]. Spatially resolved spectra of LAEs observed at $z \in (3, 6)$ with MUSE have brought unprecedented details on the structure of these distant starbursts and resolved individually their diffuse Lyα halos [37, 129]. ALMA, a recently built international facility in Chile, is an interferometer composed of 66 antennas observing at mm and sub-mm wavelengths. It is well suited for observing dusty starbursts and SMGs at $z > 2$, their distribution across redshifts, and possibly their evolution into massive early-type galaxies [130, 131]. ALMA is also efficient at mapping the distribution of dust in low-mass predecessors of MW-type galaxies, such as the UV-selected LBGs and LAEs [132] or the Chandra-detected X-ray galaxies [130]. ALMA has a sufficient sensitivity to resolve high-z infrared atomic and molecular lines that probe galaxy metallicities, ionizations and kinematics,

and determine their precise redshifts [133, 134]. In the local universe, ALMA is mapping hundreds of thousands of stellar nurseries in nearby galaxies with the goal to shed light on the star-formation mechanisms and the conditions under which the formation proceeds by intense bursts.

In the years to come, several major instruments will become active. HARMONI is a visible/NIR integral-field spectrograph in construction for the E-ELT's first light in the mid-2020s. Assisted with adaptive optics, the HARMONI angular resolution will be comparable to that achieved with space-borne instruments. The optical/NIR wavelengths will detect rest-frame UV (Lyα, continuum, lines) in the reionization era. One of the goals is the detection of Population-III stars, i.e. primordial stars with no heavy elements, possibly reaching hundreds of solar masses. Their detection through the ionized helium lines has been claimed possible with HARMONI out to $z > 10$. HARMONI will thus play an important role in probing the high-mass end of the IMF. In the local universe, HARMONI will resolve individual stars in nearby galaxies and supernovae out to $z \sim 3 - 4$, testing our models of star-formation and galaxy assembly histories. HARMONI already has a dedicated simulation tool to predict the future observational outcomes, using mock data from cosmological simulations [135]. The tool may also be an essential preparatory step for observers once the instrument is operational.

Space missions play an ever larger role in cosmic studies. The *JWST* will operate in the IR domain and will detect the rest-frame UV of reionization era galaxies. The telescope will possess the first space-borne integral-field spectrograph, NIRSPEC. Compared to the ground-based instruments, NIRSPEC will have much more severe limitations on the number of spectra that it can cover simultaneously (100 as opposed to 31,000 in HARMONI). On the other hand, it will have the advantages of the space mission, unaffected by the Earth's atmosphere. Among other future missions, ESA's *EUCLID* will map the large cosmic structure and its evolution. It will produce deep optical and NIR images and spectra of galaxies out to $z \sim 2$ across approximately half of the sky. The unprecedented extent of this catalogue will provide the basis for statistical studies mapping the galaxy assembly in the past ten billion years. In X-rays, the newly planned mission *ATHENA* will have a high sensitivity and high angular resolution. It will complete the census of evolved binary sources in starburst regions down to faint X-ray fluxes. It will resolve the spatial structure of X-ray emitting regions in galaxies and will constrain the dominant sources, discriminating between X-ray binaries, AGN, hot gas and other. Eventually, ATHENA will open the X-ray window for high-redshift galaxies, too faint to be reachable individually by current instruments.

Complementary to direct detections of starburst signatures, radio telescopes such as SKA, HERA or LOFAR will map the atomic hydrogen distribution in the universe at its different epochs, including the reionization era. Using arrays of hundreds of radio antennas, these interferometers will resolve how the neutral IGM structures evolved, in what conditions formed the first stars and galaxies and how they continue to form today.

Astronomy is experiencing a golden age and the quest for understanding how stars formed and how galaxies assembled through the cosmic history is one of its

flagships. The existing and upcoming facilities, using multiple spectral windows, take us progressively to the very first structures that formed in the universe. Supported by numerical simulations and by detailed, resolved local studies, they will complete our picture of the conditions for star formation at different epochs, the origin of galaxies as we know them today, the existence of extreme objects, and the mechanisms driving galaxy evolution.

References

1. R.C. Kennicutt Jr., Astrophys. J. **498**, 541 (1998). https://doi.org/10.1086/305588
2. F. Bigiel, A. Leroy, F. Walter, E. Brinks, W.J.G. de Blok, B. Madore, M.D. Thornley, Astron. J. **136**(6), 2846 (2008). https://doi.org/10.1088/0004-6256/136/6/2846
3. R.C. Kennicutt, N.J. Evans, Annu. Rev. Astron. Astrophys. **50**, 531 (2012). https://doi.org/10.1146/annurev-astro-081811-125610
4. R.B. Larson, B.M. Tinsley, Astrophys. J. **219**, 46 (1978). https://doi.org/10.1086/155753
5. P.A. Duc, I.F. Mirabel, Astron. Astrophys. **289**, 83 (1994)
6. S.L. Ellison, D.R. Patton, L. Simard, A.W. McConnachie, Astron. J. **135**(5), 1877 (2008). https://doi.org/10.1088/0004-6256/135/5/1877
7. P. Di Matteo, F. Combes, A.L. Melchior, B. Semelin, Astron. Astrophys. **468**(1), 61 (2007). https://doi.org/10.1051/0004-6361:20066959
8. P.F. Hopkins, E. Quataert, Mon. Not. R. Astron. Soc. **407**(3), 1529 (2010). https://doi.org/10.1111/j.1365-2966.2010.17064.x
9. B.G. Elmegreen, in *The Spectral Energy Distribution of Galaxies - SED 2011*, ed. by R.J. Tuffs, C.C. Popescu. IAU Symposium, vol. 284 (2012), pp. 317–329
10. B.G. Elmegreen, *Formation of Stars and Clusters over Cosmological Time* (2015), p. 477
11. D.M. Alexander, R.C. Hickox, New Astron. Rev. **56**(4), 93 (2012). https://doi.org/10.1016/j.newar.2011.11.003
12. H. Gerola, P.E. Seiden, Astrophys. J. **223**, 129 (1978). https://doi.org/10.1086/156243
13. T.M. Heckman, in *Starbursts: From 30 Doradus to Lyman Break Galaxies*, ed. by R. de Grijs, R.M. González Delgado. Astrophysics and Space Science Library, vol. 329 (2005), p. 3
14. N. Bergvall, Astrophys. Space Sci. Proc. **28**, 175 (2012)
15. G. Östlin, P. Amram, N. Bergvall, J. Masegosa, J. Boulesteix, I. Márquez, Astron. Astrophys. **374**, 800 (2001). https://doi.org/10.1051/0004-6361:20010832
16. N. Bergvall, T. Marquart, M.J. Way, A. Blomqvist, E. Holst, G. Östlin, E. Zackrisson, Astron. Astrophys. **587**, A72 (2016). https://doi.org/10.1051/0004-6361/201525692
17. D. Calzetti, *Star Formation Rate Indicators* (2013), p. 419
18. N.R. Walborn, J. Nichols-Bohlin, R.J. Panek, NASA Reference Publication 1155 (1985)
19. T.M. Heckman, S. Borthakur, R. Overzier, G. Kauffmann, A. Basu-Zych, C. Leitherer, K. Sembach, D.C. Martin, R.M. Rich, D. Schiminovich, M. Seibert, Astrophys. J. **730**, 5 (2011). https://doi.org/10.1088/0004-637X/730/1/5
20. J. Chisholm, C.A. Tremonti, C. Leitherer, Y. Chen, A. Wofford, B. Lundgren, Astrophys. J. **811**, 149 (2015). https://doi.org/10.1088/0004-637X/811/2/149
21. A.E. Shapley, C.C. Steidel, M. Pettini, K.L. Adelberger, Astrophys. J. **588**, 65 (2003). https://doi.org/10.1086/373922
22. B.D. Savage, K.R. Sembach, Astrophys. J. **379**, 245 (1991). https://doi.org/10.1086/170498

23. J. Chisholm, I. Orlitová, D. Schaerer, A. Verhamme, G. Worseck, Y.I. Izotov, T.X. Thuan, N.G. Guseva, Do galaxies that leak ionizing photons have extreme outflows? Astron. Astrophys. **605**, A67 (2017). https://doi.org/10.1051/0004-6361/201730610

24. S. Gazagnes, J. Chisholm, D. Schaerer, A. Verhamme, J.R. Rigby, M. Bayliss, Astron. Astrophys. **616**, A29 (2018). https://doi.org/10.1051/0004-6361/201832759

25. R.B. Partridge, P.J.E. Peebles, Astrophys. J. **147**, 868 (1967). https://doi.org/10.1086/149079

26. M. Dijkstra, Publ. Astron. Soc. Aust. **31**, e040 (2014). https://doi.org/10.1017/pasa.2014.33

27. D.L. Meier, R. Terlevich, Astrophys. J. Lett. **246**, L109 (1981). https://doi.org/10.1086/183565

28. S. Djorgovski, H. Spinrad, P. McCarthy, M.A. Strauss, Astrophys. J. Lett. **299**, L1 (1985). https://doi.org/10.1086/184569

29. D. Kunth, C. Leitherer, J.M. Mas-Hesse, G. Östlin, A. Petrosian, Astrophys. J. **597**(1), 263 (2003). https://doi.org/10.1086/378396

30. D.A. Neufeld, Astrophys. J. **350**, 216 (1990). https://doi.org/10.1086/168375

31. M. Dijkstra, Z. Haiman, M. Spaans, Astrophys. J. **649**, 14 (2006). https://doi.org/10.1086/506243

32. A. Verhamme, D. Schaerer, A. Maselli, Astron. Astrophys. **460**, 397 (2006). https://doi.org/10.1051/0004-6361:20065554

33. M. Gronke, M. Dijkstra, M. McCourt, S. Peng Oh, Resonant line transfer in a fog: using Lyman-alpha to probe tiny structures in atomic gas. Astron. Astrophys. **607**, A71 (2017). https://doi.org/10.1051/0004-6361/201731013

34. A. Verhamme, Y. Dubois, J. Blaizot, T. Garel, R. Bacon, J. Devriendt, B. Guiderdoni, A. Slyz, Astron. Astrophys. **546**, A111 (2012). https://doi.org/10.1051/0004-6361/201218783

35. M. Hayes, G. Östlin, D. Schaerer, A. Verhamme, J.M. Mas-Hesse, A. Adamo, H. Atek, J.M. Cannon, F. Duval, L. Guaita, E.C. Herenz, D. Kunth, P. Laursen, J. Melinder, I. Orlitová, H. Otí-Floranes, A. Sandberg, Astrophys. J. Lett. **765**, L27 (2013). https://doi.org/10.1088/2041-8205/765/2/L27

36. R. Momose, M. Ouchi, K. Nakajima, Y. Ono, T. Shibuya, K. Shimasaku, S. Yuma, M. Mori, M. Umemura, Mon. Not. R. Astron. Soc. **442**, 110 (2014). https://doi.org/10.1093/mnras/stu825

37. L. Wisotzki, R. Bacon, J. Blaizot, J. Brinchmann, E.C. Herenz, J. Schaye, N. Bouché, S. Cantalupo, T. Contini, C.M. Carollo, J. Caruana, J.B. Courbot, E. Emsellem, S. Kamann, J. Kerutt, F. Leclercq, S.J. Lilly, V. Patrício, C. Sandin, M. Steinmetz, L.A. Straka, T. Urrutia, A. Verhamme, P.M. Weilbacher, M. Wendt, Astron. Astrophys. **587**, A98 (2016). https://doi.org/10.1051/0004-6361/201527384

38. D. Kunth, J.M. Mas-Hesse, E. Terlevich, R. Terlevich, J. Lequeux, S.M. Fall, Astron. Astrophys. **334**, 11 (1998)

39. D. Kunth, J. Lequeux, W.L.W. Sargent, F. Viallefond, Astron. Astrophys. **282**, 709 (1994)

40. J.A. Baldwin, M.M. Phillips, R. Terlevich, Publ. Astron. Soc. Pac. **93**, 5 (1981). https://doi.org/10.1086/130766

41. G. Kauffmann, T.M. Heckman, C. Tremonti, J. Brinchmann, S. Charlot, S.D.M. White, S.E. Ridgway, J. Brinkmann, M. Fukugita, P.B. Hall, Ž. Ivezić, G.T. Richards, D.P. Schneider, Mon. Not. R. Astron. Soc. **346**(4), 1055 (2003). https://doi.org/10.1111/j.1365-2966.2003.07154.x

42. L.J. Kewley, M.A. Dopita, R.S. Sutherland, C.A. Heisler, J. Trevena, Astrophys. J. **556**, 121 (2001). https://doi.org/10.1086/321545

43. G. Stasińska, R. Cid Fernandes, A. Mateus, L. Sodré, N.V. Asari, Mon. Not. R. Astron. Soc. **371**(2), 972 (2006). https://doi.org/10.1111/j.1365-2966.2006.10732.x

44. L.J. Kewley, M.A. Dopita, C. Leitherer, R. Davé, T. Yuan, M. Allen, B. Groves, R. Sutherland, Astrophys. J. **774**, 100 (2013). https://doi.org/10.1088/0004-637X/774/2/100

45. D. Kunth, G. Östlin, Astron. Astrophys. Rev. **10**, 1 (2000). https://doi.org/10.1007/s001590000005

46. R.A. Remillard, J.E. McClintock, Annu. Rev. Astron. Astrophys. **44**(1), 49 (2006). https://doi.org/10.1146/annurev.astro.44.051905.092532

47. P. Kaaret, H. Feng, T.P. Roberts, Annu. Rev. Astron. Astrophys. **55**(1), 303 (2017). https://doi.org/10.1146/annurev-astro-091916-055259

48. J.E. Greene, J. Strader, L.C. Ho (2019). e-Prints. arXiv:1911.09678

49. T.X. Thuan, F.E. Bauer, P. Papaderos, Y.I. Izotov, Astrophys. J. **606**(1), 213 (2004). https://doi.org/10.1086/382949

50. J.P. Grimes, T. Heckman, D. Strickland, W.V. Dixon, K. Sembach, R. Overzier, C. Hoopes, A. Aloisi, A. Ptak, Feedback in the local Lyman-break Galaxy Analog Haro 11 as probed by far-ultraviolet and X-ray observations. Astrophys. J. **668**(2), 891–905 (2007). https://doi.org/10.1086/521353

51. H. Otí-Floranes, J.M. Mas-Hesse, E. Jiménez-Bailón, D. Schaerer, M. Hayes, G. Östlin, H. Atek, D. Kunth, Astron. Astrophys. **546**, A65 (2012). https://doi.org/10.1051/0004-6361/201219318

52. H. Otí-Floranes, J.M. Mas-Hesse, E. Jiménez-Bailón, D. Schaerer, M. Hayes, G. Östlin, H. Atek, D. Kunth, Astron. Astrophys. **566**, A38 (2014). https://doi.org/10.1051/0004-6361/201323069

53. A.R. Basu-Zych, B.D. Lehmer, A.E. Hornschemeier, T.S. Gonçalves, T. Fragos, T.M. Heckman, R.A. Overzier, A.F. Ptak, D. Schiminovich, Astrophys. J. **774**, 152 (2013). https://doi.org/10.1088/0004-637X/774/2/152

54. M. Brorby, P. Kaaret, Mon. Not. R. Astron. Soc. **470**(1), 606 (2017). https://doi.org/10.1093/mnras/stx1286

55. J. Svoboda, V. Douna, I. Orlitová, M. Ehle, Astrophys. J. **880**(2), 144 (2019). https://doi.org/10.3847/1538-4357/ab2b39

56. P. Ranalli, A. Comastri, G. Setti, Astron. Astrophys. **399**, 39 (2003). https://doi.org/10.1051/0004-6361:20021600

57. V.M. Douna, L.J. Pellizza, I.F. Mirabel, S.E. Pedrosa, Astron. Astrophys. **579**, A44 (2015). https://doi.org/10.1051/0004-6361/201525617

58. M. Brorby, P. Kaaret, A. Prestwich, I.F. Mirabel, Mon. Not. R. Astron. Soc. **457**(4), 4081 (2016). https://doi.org/10.1093/mnras/stw284

59. M. Cerviño, J.M. Mas-Hesse, D. Kunth, Astron. Astrophys. **392**, 19 (2002). https://doi.org/10.1051/0004-6361:20020785

60. J.M. Mas-Hesse, H. Otí-Floranes, M. Cerviño, Astron. Astrophys. **483**(1), 71 (2008). https://doi.org/10.1051/0004-6361:20078398

61. S. Mineo, M. Gilfanov, B.D. Lehmer, G.E. Morrison, R. Sunyaev, Mon. Not. R. Astron. Soc. **437**, 1698 (2014). https://doi.org/10.1093/mnras/stt1999

62. F. Zwicky, Astrophys. J. **142**, 1293 (1965). https://doi.org/10.1086/148411

63. W.L.W. Sargent, Astrophys. J. **160**, 405 (1970). https://doi.org/10.1086/150443

64. R. Terlevich, J. Melnick, J. Masegosa, M. Moles, M.V.F. Copetti, Astron. Astrophys. Suppl. Ser. **91**, 285 (1991)

65. I. Gallagher, S. John, D.A. Hunter, Astron. J. **94**, 43 (1987). https://doi.org/10.1086/114445

66. L. Searle, W.L.W. Sargent, Astrophys. J. **173**, 25 (1972). https://doi.org/10.1086/151398

67. M. Hayes, Publ. Astron. Soc. Aust. **32**, e027 (2015). https://doi.org/10.1017/pasa.2015.25

68. G. Östlin, M. Hayes, F. Duval, A. Sandberg, T. Rivera-Thorsen, T. Marquart, I. Orlitová, A. Adamo, J. Melinder, L. Guaita, H. Atek, J.M. Cannon, P. Gruyters, E.C. Herenz, D. Kunth, P. Laursen, J.M. Mas-Hesse, G. Micheva, H. Otí-Floranes, S.A. Pardy, M.M. Roth, D. Schaerer, A. Verhamme, Astrophys. J. **797**, 11 (2014). https://doi.org/10.1088/0004-637X/797/1/11

69. T.E. Rivera-Thorsen, M. Hayes, G. Östlin, F. Duval, I. Orlitová, A. Verhamme, J.M. Mas-Hesse, D. Schaerer, J.M. Cannon, H. Otí-Floranes, A. Sandberg, L. Guaita, A. Adamo, H. Atek, E.C. Herenz, D. Kunth, P. Laursen, J. Melinder, Astrophys. J. **805**, 14 (2015). https://doi.org/10.1088/0004-637X/805/1/14

70. E.C. Herenz, P. Gruyters, I. Orlitova, M. Hayes, G. Östlin, J.M. Cannon, M.M. Roth, A. Bik, S. Pardy, H. Otí-Floranes, J.M. Mas-Hesse, A. Adamo, H. Atek, F. Duval, L. Guaita, D. Kunth, P. Laursen, J. Melinder, J. Puschnig, T.E. Rivera-Thorsen, D. Schaerer, A. Verhamme, Astron. Astrophys. **587**, A78 (2016). https://doi.org/10.1051/0004-6361/201527373

71. S.A. Pardy, J.M. Cannon, G. Östlin, M. Hayes, T. Rivera-Thorsen, A. Sandberg, A. Adamo, E. Freeland, E.C. Herenz, L. Guaita, D. Kunth, P. Laursen, J.M. Mas-Hesse, J. Melinder, I. Orlitová, H. Otí-Floranes, J. Puschnig, D. Schaerer, A. Verhamme, Astrophys. J. **794**, 101 (2014). https://doi.org/10.1088/0004-637X/794/2/101

72. T.M. Heckman, C.G. Hoopes, M. Seibert, D.C. Martin, S. Salim, R.M. Rich, G. Kauffmann, S. Charlot, T.A. Barlow, L. Bianchi, Y.I. Byun, J. Donas, K. Forster, P.G. Friedman, P.N. Jelinsky, Y.W. Lee, B.F. Madore, R.F. Malina, B. Milliard, P.F. Morrissey, S.G. Neff, D. Schiminovich, O.H.W. Siegmund, T. Small, A.S. Szalay, B.Y. Welsh, T.K. Wyder, Astrophys. J. Lett. **619**(1), L35 (2005). https://doi.org/10.1086/425979

73. A.R. Basu-Zych, B. Lehmer, T. Fragos, A. Hornschemeier, M. Yukita, A. Zezas, A. Ptak, Astrophys. J. **818**(2), 140 (2016). https://doi.org/10.3847/0004-637X/818/2/140

74. E. Leitet, N. Bergvall, M. Hayes, S. Linné, E. Zackrisson, Astron. Astrophys. **553**, A106 (2013). https://doi.org/10.1051/0004-6361/201118370

75. C. Cardamone, K. Schawinski, M. Sarzi, S.P. Bamford, N. Bennert, C.M. Urry, C. Lintott, W.C. Keel, J. Parejko, R.C. Nichol, D. Thomas, D. Andreescu, P. Murray, M.J. Raddick, A. Slosar, A. Szalay, J. Vandenberg, Mon. Not. R. Astron. Soc. **399**, 1191 (2009). https://doi.org/10.1111/j.1365-2966.2009.15383.x

76. Y.I. Izotov, N.G. Guseva, T.X. Thuan, Astrophys. J. **728**, 161 (2011). https://doi.org/10.1088/0004-637X/728/2/161

77. A.E. Jaskot, M.S. Oey, Astrophys. J. **766**, 91 (2013). https://doi.org/10.1088/0004-637X/766/2/91

78. A. Henry, C. Scarlata, C.L. Martin, D. Erb, Astrophys. J. **809**, 19 (2015). https://doi.org/10.1088/0004-637X/809/1/19

79. H. Yang, S. Malhotra, M. Gronke, J.E. Rhoads, C. Leitherer, A. Wofford, T. Jiang, M. Dijkstra, V. Tilvi, J. Wang, Astrophys. J. **844**(2), 171 (2017). https://doi.org/10.3847/1538-4357/aa7d4d

80. I. Orlitová, A. Verhamme, A. Henry, C. Scarlata, A. Jaskot, M.S. Oey, D. Schaerer, Astron. Astrophys. **616**, A60 (2018). https://doi.org/10.1051/0004-6361/201732478

81. Y.I. Izotov, G. Worseck, D. Schaerer, N.G. Guseva, T.X. Thuan, Fricke, A. Verhamme, I. Orlitová, Mon. Not. R. Astron. Soc. **478**(4), 4851 (2018). https://doi.org/10.1093/mnras/sty1378

82. Y.I. Izotov, I. Orlitová, D. Schaerer, T.X. Thuan, A. Verhamme, N.G. Guseva, G. Worseck, Nature **529**, 178 (2016). https://doi.org/10.1038/nature16456

83. T. Kawamuro, Y. Ueda, K. Ichikawa, M. Imanishi, T. Izumi, A. Tanimoto, K. Matsuoka, Astrophys. J. **881**(1), 48 (2019). https://doi.org/10.3847/1538-4357/ab2bf6

84. A.W. Blain, I. Smail, R.J. Ivison, J.P. Kneib, D.T. Frayer, Phys. Rep. **369**(2), 111 (2002). https://doi.org/10.1016/S0370-1573(02)00134-5

85. C.J. Lonsdale, D. Farrah, H.E. Smith, in *Ultraluminous Infrared Galaxies* (2006), p. 285

86. C.M. Casey, D. Narayanan, A. Cooray, Phys. Rep. **541**(2), 45 (2014). https://doi.org/10.1016/j.physrep.2014.02.009

87. C. Leitherer, R. Chandar, C.A. Tremonti, A. Wofford, D. Schaerer, Astrophys. J. **772**, 120 (2013). https://doi.org/10.1088/0004-637X/772/2/120

88. C.C. Steidel, M. Giavalisco, M. Dickinson, K.L. Adelberger, Astron. J. **112**, 352 (1996). https://doi.org/10.1086/118019

89. B. Vulcani, M. Trenti, V. Calvi, R. Bouwens, P. Oesch, M. Stiavelli, M. Franx, Characterization and modeling of contamination for Lyman break galaxy samples at high redshift. Astrophys. J. **836**(2), 239 (2017). https://doi.org/10.3847/1538-4357/aa5caf

90. A.M. Quider, M. Pettini, A.E. Shapley, C.C. Steidel, Mon. Not. R. Astron. Soc. **398**, 1263 (2009). https://doi.org/10.1111/j.1365-2966.2009.15234.x

91. A.M. Quider, A.E. Shapley, M. Pettini, C.C. Steidel, D.P. Stark, Mon. Not. R. Astron. Soc. **402**, 1467 (2010). https://doi.org/10.1111/j.1365-2966.2009.16005.x

92. M. Dessauges-Zavadsky, S. D'Odorico, D. Schaerer, A. Modigliani, C. Tapken, J. Vernet, Astron. Astrophys. **510**, A26 (2010). https://doi.org/10.1051/0004-6361/200913337

93. T.E. Rivera-Thorsen, H. Dahle, M. Gronke, M. Bayliss, J.R. Rigby, R. Simcoe, R. Bordoloi, M. Turner, G. Furesz, Astron. Astrophys. **608**, L4 (2017). https://doi.org/10.1051/0004-6361/201732173

94. M. Giavalisco, Annu. Rev. Astron. Astrophys. **40**, 579 (2002). https://doi.org/10.1146/annurev.astro.40.121301.111837

95. J.S. Dunlop, in *Observing the First Galaxies*. Astrophysics and Space Science Library, vol. 396 (2013), p. 223

96. C. Behrens, M. Dijkstra, J.C. Niemeyer, Astron. Astrophys. **563**, A77 (2014). https://doi.org/10.1051/0004-6361/201322949

97. A. Verhamme, I. Orlitová, D. Schaerer, M. Hayes, Astron. Astrophys. **578**, A7 (2015). https://doi.org/10.1051/0004-6361/201423978

98. A. Hagen, G.R. Zeimann, C. Behrens, R. Ciardullo, H.S. Grasshorn Gebhardt, C. Gronwall, J.S. Bridge, D.B. Fox, D.P. Schneider, J.R. Trump, G.A. Blanc, Y.K. Chiang, T.S. Chonis, S.L. Finkelstein, G.J. Hill, S. Jogee, E. Gawiser, Astrophys. J. **817**, 79 (2016). https://doi.org/10.3847/0004-637X/817/1/79

99. M. Ouchi, B. Mobasher, K. Shimasaku, H.C. Ferguson, S.M. Fall, Y. Ono, N. Kashikawa, T. Morokuma, K. Nakajima, S. Okamura, M. Dickinson, M. Giavalisco, K. Ohta, Astrophys. J. **706**, 1136 (2009). https://doi.org/10.1088/0004-637X/706/2/1136

100. M. Hayes, D. Schaerer, G. Östlin, J.M. Mas-Hesse, H. Atek, D. Kunth, Astrophys. J. **730**(1), 8 (2011). https://doi.org/10.1088/0004-637X/730/1/8

101. H. Atek, D. Kunth, D. Schaerer, J.M. Mas-Hesse, M. Hayes, G. Östlin, J.P. Kneib, Astron. Astrophys. **561**, A89 (2014). https://doi.org/10.1051/0004-6361/201321519

102. D. Sobral, J. Matthee, B. Darvish, D. Schaerer, B. Mobasher, H.J.A. Röttgering, S. Santos, S. Hemmati, Astrophys. J. **808**, 139 (2015). https://doi.org/10.1088/0004-637X/808/2/139

103. A. Zitrin, I. Labbé, S. Belli, R. Bouwens, R.S. Ellis, G. Roberts-Borsani, D.P. Stark, P.A. Oesch, R. Smit, Astrophys. J. Lett. **810**, L12 (2015). https://doi.org/10.1088/2041-8205/810/1/L12

104. P.A. Oesch, G. Brammer, P.G. van Dokkum, G.D. Illingworth, R.J. Bouwens, I. Labbé, M. Franx, I. Momcheva, M.L.N. Ashby, G.G. Fazio, V. Gonzalez, B. Holden, D. Magee, R.E. Skelton, R. Smit, L.R. Spitler, M. Trenti, S.P. Willner, Astrophys. J. **819**, 129 (2016). https://doi.org/10.3847/0004-637X/819/2/129

105. L. Guaita, E. Gawiser, N. Padilla, H. Francke, N.A. Bond, C. Gronwall, R. Ciardullo, J.J. Feldmeier, S. Sinawa, G.A. Blanc, S. Virani, Astrophys. J. **714**, 255 (2010). https://doi.org/10.1088/0004-637X/714/1/255

106. J.D. Bowman, A.E.E. Rogers, R.A. Monsalve, T.J. Mozdzen, N. Mahesh, Nature **555**(7694), 67 (2018). https://doi.org/10.1038/nature25792

107. J.E. Gunn, B.A. Peterson, Astrophys. J. **142**, 1633 (1965). https://doi.org/10.1086/148444

108. G.D. Becker, J.S. Bolton, A. Lidz, Publ. Astron. Soc. Aust. **32**, e045 (2015). https://doi.org/10.1017/pasa.2015.45

109. B.E. Robertson, S.R. Furlanetto, E. Schneider, S. Charlot, R.S. Ellis, D.P. Stark, R.J. McLure, J.S. Dunlop, A. Koekemoer, M.A. Schenker, M. Ouchi, Y. Ono, E. Curtis-Lake, A.B. Rogers, R.A.A. Bowler, M. Cirasuolo, Astrophys. J. **768**(1), 71 (2013). https://doi.org/10.1088/0004-637X/768/1/71

110. B.E. Robertson, R.S. Ellis, S.R. Furlanetto, J.S. Dunlop, Astrophys. J. Lett. **802**(2), L19 (2015). https://doi.org/10.1088/2041-8205/802/2/L19

111. B.E. Robertson, R.S. Ellis, J.S. Dunlop, R.J. McLure, D.P. Stark, Nature **468**(7320), 49 (2010). https://doi.org/10.1038/nature09527

112. J.P. Paardekooper, S. Khochfar, C. Dalla Vecchia, Mon. Not. R. Astron. Soc. **451**, 2544 (2015)

113. S. Borthakur, T.M. Heckman, C. Leitherer, R.A. Overzier, Science **346**, 216 (2014). https://doi.org/10.1126/science.1254214

114. E. Vanzella, S. de Barros, K. Vasei, A. Alavi, M. Giavalisco, B. Siana, A. Grazian, G. Hasinger, H. Suh, N. Cappelluti, F. Vito, R. Amorin, I. Balestra, M. Brusa, F. Calura, M. Castellano, A. Comastri, A. Fontana, R. Gilli, M. Mignoli, L. Pentericci, C. Vignali, G. Zamorani, Astrophys. J. **825**, 41 (2016). https://doi.org/10.3847/0004-637X/825/1/41

115. A.E. Shapley, C.C. Steidel, A.L. Strom, M. Bogosavljević, N.A. Reddy, B. Siana, R.E. Mostardi, G.C. Rudie, Q1549-C25: a clean source of Lyman-continuum emission at z = 3.15. Astrophys. J. **826**(2), L24 (2016). https://doi.org/10.3847/2041-8205/826/2/L24

116. F. Bian, X. Fan, I. McGreer, Z. Cai, L. Jiang, Astrophys. J. Lett. **837**, L12 (2017). https://doi.org/10.3847/2041-8213/aa5ff7

117. C.C. Steidel, M. Bogosavljević, A.E. Shapley, N.A. Reddy, G.C. Rudie, M. Pettini, R.F. Trainor, A.L. Strom, Astrophys. J. **869**(2), 123 (2018). https://doi.org/10.3847/1538-4357/aaed28

118. T.J. Fletcher, M. Tang, B.E. Robertson, K. Nakajima, R.S. Ellis, D.P. Stark, A. Inoue, Astrophys. J. **878**(2), 87 (2019). https://doi.org/10.3847/1538-4357/ab2045

119. K. Nakajima, M. Ouchi, Mon. Not. R. Astron. Soc. **442**, 900 (2014). https://doi.org/10.1093/mnras/stu902

120. G. Stasińska, Y. Izotov, C. Morisset, N. Guseva, Astron. Astrophys. **576**, A83 (2015). https://doi.org/10.1051/0004-6361/201425389

121. J. Chisholm, S. Gazagnes, D. Schaerer, A. Verhamme, J.R. Rigby, M. Bayliss, K. Sharon, M. Gladders, H. Dahle, Astron. Astrophys. **616**, A30 (2018). https://doi.org/10.1051/0004-6361/201832758

122. A. Verhamme, I. Orlitová, D. Schaerer, Y. Izotov, G. Worseck, T.X. Thuan, N. Guseva, Astron. Astrophys. **597**, A13 (2017). https://doi.org/10.1051/0004-6361/201629264

123. E. Giallongo, A. Grazian, F. Fiore, A. Fontana, L. Pentericci, E. Vanzella, M. Dickinson, D. Kocevski, M. Castellano, S. Cristiani, H. Ferguson, S. Finkelstein, N. Grogin, N. Hathi, A.M. Koekemoer, J.A. Newman, M. Salvato, Astron. Astrophys. **578**, A83 (2015). https://doi.org/10.1051/0004-6361/201425334

124. P. Madau, F. Haardt, Astrophys. J. Lett. **813**(1), L8 (2015). https://doi.org/10.1088/2041-8205/813/1/L8

125. S. Mitra, T.R. Choudhury, A. Ferrara, Mon. Not. R. Astron. Soc. **473**(1), 1416 (2018). https://doi.org/10.1093/mnras/stx2443

126. N. Trentham, in *Starbursts: From 30 Doradus to Lyman Break Galaxies*, ed. by R. de Grijs, R.M. González Delgado. Astrophysics and Space Science Library, vol. 329 (2005), p. 115

127. R. Bacon, J. Brinchmann, J. Richard, T. Contini, A. Drake, M. Franx, S. Tacchella, J. Vernet, L. Wisotzki, J. Blaizot, N. Bouché, R. Bouwens, S. Cantalupo, C.M. Carollo, D. Carton, J. Caruana, B. Clément, S. Dreizler, B. Epinat, B. Guiderdoni, C. Herenz, T.O. Husser, S. Kamann, J. Kerutt, W. Kollatschny, D. Krajnovic, S. Lilly, T. Martinsson, L. Michel-Dansac, V. Patricio, J. Schaye, M. Shirazi, K. Soto, G. Soucail, M. Steinmetz, T. Urrutia, P. Weilbacher, T. de Zeeuw, Astron. Astrophys. **575**, A75 (2015). https://doi.org/10.1051/0004-6361/201425419

128. R. Bacon, S. Conseil, D. Mary, J. Brinchmann, M. Shepherd, M. Akhlaghi, P.M. Weilbacher, L. Piqueras, L. Wisotzki, D. Lagattuta, B. Epinat, A. Guerou, H. Inami, S. Cantalupo, J.B. Courbot, T. Contini, J. Richard, M. Maseda, R. Bouwens, N. Bouché, W. Kollatschny, J. Schaye, R.A. Marino, R. Pello, C. Herenz, B. Guiderdoni, M. Carollo, Astron. Astrophys. **608**, A1 (2017). https://doi.org/10.1051/0004-6361/201730833

129. L. Wisotzki, R. Bacon, J. Brinchmann, S. Cantalupo, P. Richter, J. Schaye, K.B. Schmidt, T. Urrutia, P.M. Weilbacher, M. Akhlaghi, N. Bouché, T. Contini, B. Guiderdoni, E.C. Herenz, H. Inami, J. Kerutt, F. Leclercq, R.A. Marino, M. Maseda, A. Monreal-Ibero, T. Nanayakkara, J. Richard, R. Saust, M. Steinmetz, M. Wendt, Nature **562**(7726), 229 (2018). https://doi.org/10.1038/s41586-018-0564-6

130. A. Karim, A.M. Swinbank, J.A. Hodge, I.R. Smail, F. Walter, A.D. Biggs, J.M. Simpson, A.L.R. Danielson, D.M. Alexander, F. Bertoldi, C. de Breuck, S.C. Chapman, K.E.K. Coppin, H. Dannerbauer, A.C. Edge, T.R. Greve, R.J. Ivison, K.K. Knudsen, K.M. Menten, E. Schinnerer, J.L. Wardlow, A. Weiß, P. van der Werf, Mon. Not. R. Astron. Soc. **432**(1), 2 (2013). https://doi.org/10.1093/mnras/stt196

131. J.S. Dunlop, R.J. McLure, A.D. Biggs, J.E. Geach, M.J. Michałowski, R.J. Ivison, W. Rujopakarn, E. van Kampen, A. Kirkpatrick, A. Pope, D. Scott, A.M. Swinbank, T.A. Targett, I. Aretxaga, J.E. Austermann, P.N. Best, V.A. Bruce, E.L. Chapin, S. Charlot,

M. Cirasuolo, K. Coppin, R.S. Ellis, S.L. Finkelstein, C.C. Hayward, D.H. Hughes, E. Ibar, P. Jagannathan, S. Khochfar, M.P. Koprowski, D. Narayanan, K. Nyland, C. Papovich, J.A. Peacock, G.H. Rieke, B. Robertson, T. Vernstrom, P.P.v.d. Werf, G.W. Wilson, M. Yun, Mon. Not. R. Astron. Soc. **466**(1), 861 (2017). https://doi.org/10.1093/mnras/stw3088

132. D.A. Riechers, A. Pope, E. Daddi, L. Armus, C.L. Carilli, F. Walter, J. Hodge, R.R. Chary, G.E. Morrison, M. Dickinson, H. Dannerbauer, D. Elbaz, Astrophys. J. **786**(1), 31 (2014). https://doi.org/10.1088/0004-637X/786/1/31

133. J.D. Vieira, D.P. Marrone, S.C. Chapman, C. De Breuck, Y.D. Hezaveh, A. Weiβ, J.E. Aguirre, K.A. Aird, M. Aravena, M.L.N. Ashby, M. Bayliss, B.A. Benson, A.D. Biggs, L.E. Bleem, J.J. Bock, M. Bothwell, C.M. Bradford, M. Brodwin, J.E. Carlstrom, C.L. Chang, T.M. Crawford, A.T. Crites, T. de Haan, M.A. Dobbs, E.B. Fomalont, C.D. Fassnacht, E.M. George, M.D. Gladders, A.H. Gonzalez, T.R. Greve, B. Gullberg, N.W. Halverson, F.W. High, G.P. Holder, W.L. Holzapfel, S. Hoover, J.D. Hrubes, T.R. Hunter, R. Keisler, A.T. Lee, E.M. Leitch, M. Lueker, D. Luong-van, M. Malkan, V. McIntyre, J.J. McMahon, J. Mehl, K.M. Menten, S.S. Meyer, L.M. Mocanu, E.J. Murphy, T. Natoli, S. Padin, T. Plagge, C.L. Reichardt, A. Rest, J. Ruel, J.E. Ruhl, K. Sharon, K.K. Schaffer, L. Shaw, E. Shirokoff, J.S. Spilker, B. Stalder, Z. Staniszewski, A.A. Stark, K. Story, K. Vanderlinde, N. Welikala, R. Williamson, Nature **495**, 344 (2013). https://doi.org/10.1038/nature12001

134. T. Hashimoto, N. Laporte, K. Mawatari, R.S. Ellis, A.K. Inoue, E. Zackrisson, G. Roberts-Borsani, W. Zheng, Y. Tamura, F.E. Bauer, T. Fletcher, Y. Harikane, B. Hatsukade, N.H. Hayatsu, Y. Matsuda, H. Matsuo, T. Okamoto, M. Ouchi, R. Pelló, C.E. Rydberg, I. Shimizu, Y. Taniguchi, H. Umehata, N. Yoshida, Nature **557**, 392 (2018). https://doi.org/10.1038/s41586-018-0117-z

135. R. Augustin, S. Quiret, B. Milliard, C. Péroux, D. Vibert, J. Blaizot, Y. Rasera, R. Teyssier, S. Frank, J.M. Deharveng, V. Picouet, D.C. Martin, E.T. Hamden, N. Thatte, M. Pereira Santaella, L. Routledge, S. Zieleniewski, Mon. Not. R. Astron. Soc. **489**(2), 2417 (2019). https://doi.org/10.1093/mnras/stz2238